Multi-UAV Collaborative Trajectory Optimization for Asynchronous 3-D Passive Multitarget Tracking

Jinhui Dai, Wenqiang Pu, *Member, IEEE*, Junkun Yan, *Senior Member, IEEE*, Qingjiang Shi, *Member, IEEE*, and Hongwei Liu, *Senior Member, IEEE*

***Abstract*— This article considers the 3-D collaborative trajectory optimization (CTO) of multiple unmanned aerial vehicles to improve multitarget tracking performance with an asynchronous angle of arrival measurements. The predicted conditional Cramér–Rao lower bound is adopted as a performance measure to predict and subsequently control tracking error online. Then, the CTO problem is cast as a time-varying nonconvex problem subjected to constraints arising from dynamic and security (height, collision, and obstacle/target/threat avoidance). Finally, a comprehensive solution method (CSM) is presented to tackle the resulting problem, according to its unique structures. Specifically, if all security constraints are inactive, the CTO can be simplified as a nonconvex problem with convex dynamic constraints, which can be solved by the nonmonotone spectral projected gradient (NSPG) method. Oppositely, an alternating direction penalty method (ADPM) is presented to solve the CTO problem with some positive security constraints. The ADPM introduces auxiliary vectors to decouple the complex constraints and separates the CTO into several subproblems and tackles them alternately, while locally adjusting the penalty factor at each iteration. We show the subproblem w.r.t. the position vector is nonconvex but with convex constraints, which can be efficiently solved by the NSPG method. The subproblems w.r.t. the auxiliary vectors are separable and have closed-form solutions. Simulation results demonstrate that the CSM outperforms the unoptimized method in terms of tracking performance. Besides, the CSM achieves the near-optimal performance provided by the genetic algorithm with much lower computational complexity.**

***Index Terms*— Asynchronous target tracking, passive sensor, resource allocation, trajectory optimization (TO), unmanned aerial vehicle (UAV).**

Manuscript received 29 October 2022; revised 13 December 2022; accepted 17 January 2023. Date of publication 26 January 2023; date of current version 3 February 2023. This work was supported in part by the National Natural Science Foundation of China under Grant 62101350, Grant 62071345, and Grant 62192714; in part by the Fund for Foreign Scholars in University Research and Teaching Programs (111 Project) under Grant B18039; in part by the Aeronautical Science Foundation of China under Grant 201920081002; and in part by the Foundation of National Radar Signal Processing Laboratory under Grant 61424010406. *(Corresponding authors: Junkun Yan; Wenqiang Pu.)*

Jinhui Dai, Junkun Yan, and Hongwei Liu are with the National Laboratory of Radar Signal Processing, Xidian University, Xi'an 710071, China (e-mail: jhdai_18@stu.xidian.edu.cn; jkyan@xidian.edu.cn; hwliu@xidian.edu.cn).

Wenqiang Pu is with the Shenzhen Research Institute of Big Data, Shenzhen 518172, China (e-mail: wenqiangpu@cuhk.edu.cn).

Qingjiang Shi is with the School of Software Engineering, Tongji University, Shanghai 201804, China, and also with the Shenzhen Research Institute of Big Data, Shenzhen 518172, China (e-mail: shiqj@tongji.edu.cn).

Digital Object Identifier 10.1109/TGRS.2023.3239952

I. Introduction

A. Motivation and Related Work

TRAJECTORY optimization (TO) aims to predetermine the waypoints of unmanned aerial vehicles (UAVs) to achieve various tasks, such as minimizing fuel/battery consumption [1], maximizing search area coverage [2], or improving localization/tracking performance [3], [4], and so on. Passive tracking of radio emitters/targets with UAVs is among these tasks, which has wide applications in military and civilian fields, including target tracking in electronic reconnaissance and mobile user tracking in a wireless communication network [5] and so on. The sensing capabilities of UAVs depend not only on the measurement quality of payload passive sensors but also on the geometry of multi-UAV [6]. Therefore, one of the main research challenges is how to automatically optimize the trajectories of UAVs online to maximize tracking accuracy while simultaneously meeting the constraints deriving from speed, turning angle, height, collision, and obstacle avoidance.

To tackle this challenge, several TO models and corresponding solution algorithms are proposed for target localization/tracking in [7], [8], [9], [10], [11], [12], [13], [14], [15], [16], [17], [18], [19], [20], [21], [22], [23], [24], [25], [26]. Tzoreff and Weiss [7] discuss online and offline TO problems for a single UAV in the presence of time of arrival (TOA) measurements, subject to speed and no-fly zone constraints. The proximal policy method and the policy rollout algorithm are applied to TO problems to speed up the localization of an emitter with angle of arrival (AOA) measurements in [8] and [9], respectively. These TO schemes for single-UAV [7], [8], [9] do not require consideration of collision avoidance and communication distance constraints, whereas these constraints should be considered in multi-UAV collaborative TO (CTO) problems [10], [11], [12], [13], [14]. A receiver TO problem subjected to the minimal distance allowed to the emitter is considered in [10] to improve the localization performance, which is solved by the projected gradient (PG) method. Then, Dogancay [10] extends their work to a multitarget localization environment [11]. In [12], a steering control approach is proposed for a pair of UAVs in the time difference of arrival (TDOA)-based localization of a single emitter. In [13], a noncausal TO scheme is addressed for the received signal strength (RSS)-based localization to obtain

a higher final localization accuracy. A TO problem for multiple UAVs with heterogeneous payload sensors is considered in [14] to maximize the localization performance of an emitter while avoiding threats and ensuring effective communication between UAVs. However, the previous works [10], [11], [12], [13], [14] only optimize the steering of multi-UAV and do not take full advantage of the degree of freedom concerning speed.

An offline 2-D TO problem for a single-emitter location utilizing two moving AOA sensors is considered in [15] to improve the localization performance. In this article, the TO is formulated as a semidefinite programming problem with several constraints rising from dynamic, collision, and obstacle limitations, which is tackled by the alternating direction method of multipliers [27] (ADMM). However, this work [15] assumes a constant covariance of the measurement noise, but it decreases as the UAV approaches the target in practice. Besides, the convergence of ADMM for solving nonconvex problems is related to initial points and penalty factors, tuning of these parameters is needed for a good performance. The adjustment of these parameters relies on experience and is scenario-dependent.

Different from localization tasks, a prediction dynamic model should be considered in tracking applications, which would expand the uncertainty in the state estimation over time due to the target motion. Hernandez [16] addresses an unconstrained TO problem for AOA sensors mounted on multiple UAV platforms and proposes a quadrant search method that iteratively restricts the search to the most promising quadrant. In [17], [18], [19], [20], several joint TO and resource allocation problems are investigated to improve tracking accuracy, which is solved by the cyclic minimization-based methods and genetic algorithm (GA). A CTO problem is considered in [21] to track a moving emitter using RSS sensors, which is solved by the model predictive method. In [22], a centralized steering optimization scheme is presented for a pair of UAVs to improve tracking accuracy. For the same purpose, a heuristic planner is proposed in [23] to guide the waypoints of multi-UAV while avoiding no-fly zones. However, collision and obstacle avoidance is not fully investigated in [16], [17], [18], [19], [20], [21], [22], [23]. The TO problem is formulated in a partially observable Markov decision process framework in [24], where the goal is to improve tracking performance while achieving threat and collision avoidance. A CTO problem is addressed in [25] to minimize the overall tracking error of multiple emitters while avoiding no-fly zones. This work assumes that each UAV simultaneously intercepts signals from multiple emitters. However, the transmit signals are usually asynchronous across multiple emitters in practice.

Most of the previous works [7], [8], [9], [10], [11], [12], [13], [14], [15], [16], [17], [18], [19], [20], [21], [22], [23], [24], [25] focus on 2-D TO. On the one hand, the 2-D TO ignores the possibility of exploiting the altitude dimension to improve tracking performance. On the other hand, the increased dimensions of variables and the intercoupling of multiple nonconvex constraints make the online 3-D CTO problem more challenging. A 3-D CTO problem subject to communication range and no-fly zone constraints is considered in [26] for target tracking. In this work [26], the 3-D trajectories are decomposed into two 2-D trajectories in the horizontal and vertical directions and optimized by gradient-descent and grid search methods, respectively. The premise of this decomposition technique is that the velocity constraints in the horizontal and vertical directions are not coupled. This assumption may not hold for some types of UAVs, such as fixed-wing UAVs. In addition, the proposed model in [26] is not suitable for multiple target tracking (MTT) problems.

B. Main Contributions

This article considers a 3-D CTO for multi-UAV armed with AOA sensors[1] in asynchronous passive MTT environments. The major contributions are threefold:

1) *A closed-loop asynchronous tracking framework is built for CTO*. In this framework, the maximum likelihood (ML) estimator [28] is applied to obtain the composite measurement (CM) from the current AOA measurements spanning the fusion time interval. Then, the CMs are processed by the Kalman filter (KF) to estimate and predict the states of multiple targets [29]. According to the prediction information, we calculate the predicted conditional Cramér–Rao lower bound (PC-CRLB) and adopt it as a performance measure to precontrol the tracking error online [30]. Finally, the waypoints are optimized in the fusion center and then fed back to multiple UAVs
2) *To improve the overall MTT performance with asynchronous AOA measurements, we model the 3-D CTO as a time-varying nonconvex problem subjected to dynamic and security constraints*. Since the arrival time of measurements from different targets w.r.t. each sensor is random, existing researches [7], [8], [9], [10], [11], [12], [13], [14], [15], [16], [17], [18], [19], [20], [21], [22], [23], [24], [25], [26] cannot be applied to the 3-D CTO problem in the passive MTT context. We introduce the fusion time interval for time alignment and implement CTO in each fusion time instant. The dynamic constraints deriving from the speed and turning angle are represented as convex sets. The time-varying security constraints arising from the height, collision, and obstacle avoidance may not work at some time instants, leading to the formulation of the 3-D CTO as a time-varying nonconvex problem, since the PC-CRLB is nonconvex w.r.t. waypoints of multi-UAV.
3) *A fast comprehensive solution method (CSM) incorporates the nonmonotone spectral PG (NSPG) method and the alternating direction penalty method (ADPM) is proposed to solve the CTO problem, by exploring its time-varying characteristic*. The CSM begins with a judgment of which security constraints are active. If all security constraints are inactive, the CTO can be reduced to a nonconvex optimization problem with convex dynamic constraints, which can be efficiently solved by the NSPG

[1]Compared with TOA, TDOA, and RSS, AOA does not require synchronization with the emitter or among the receivers and is insensitive to channel variation.

method [31] with the proposed closed-form projection operator. In the case that some security constraints may be activated during the CTO process, we introduce some auxiliary vectors for the positive security constraints to decouple them. Then, we reformulate the CTO as an equality-constrained nonconvex optimization problem, which can be handled by the ADPM framework [27]. The ADPM separates the CTO into several subproblems, which can be tackled by the NSPG method or have closed-form solutions.

The remainder of this article is organized as follows. The system description is given in Section II. A two-step method for passive MTT with asynchronous AOA measurements is introduced in Section III. The formulation of the CTO scheme and the corresponding solution technique are presented in Section IV. Several simulation results are analyzed in Section V to demonstrate the effectiveness of the CSM. Finally, Section VI concludes this article.

II. System Description

A potential scenario of multi-UAV multitarget tracking is shown in Fig. 1, where Q widely separated point targets are considered to be tracked by N UAVs. Each UAV is equipped with a passive sensor that can intercept the signal emitted by multiple targets and provide AOA measurements. Note that the signal launch time of multitarget is different, leading to the measurement arrival time for different targets w.r.t. each sensor is asynchronous, details are presented in Section II-C. To collaboratively track multiple targets, a fusion time interval T_0 is specified for simultaneous multitarget tracking in CTO. At the fusion time instant t_k ($t_k = t_{k-1} + T_0$), the position $\mathbf{x}_{q,k}^p = (x_{q,k}, y_{q,k}, z_{q,k})^T$ and the velocity $\mathbf{x}_{q,k}^v = (\dot{x}_{q,k}, \dot{y}_{q,k}, \dot{z}_{q,k})^T$ of target $q \in \{1, 2, \ldots, Q\}$ are unknown parameters to be estimated, then $\mathbf{x}_{q,k} = (x_{q,k}, \dot{x}_{q,k}, y_{q,k}, \dot{y}_{q,k}, z_{q,k}, \dot{z}_{q,k})^T$ is defined as the state of target q. The position and velocity of UAV $n \in \{1, 2, \ldots, N\}$ are $\mathbf{p}_{n,k} = (x_{n,k}, y_{n,k}, z_{n,k})^T$ and $\mathbf{v}_{n,k} = (\dot{x}_{n,k}, \dot{y}_{n,k}, \dot{z}_{n,k})^T$, respectively.

A. Dynamic Model for Target q

The dynamic of target q is described as the nearly constant velocity model [32]

$$\mathbf{x}_{q,k} = \mathbf{F}_{k-1}\mathbf{x}_{q,k-1} + \mathbf{u}_{q,k-1} \tag{1}$$

where $\mathbf{F}_{k-1}$ is the state transition matrix, and $\mathbf{u}_{q,k-1}$ is a zero-mean Gaussian process noise with covariance $\mathbf{Q}_{q,k-1}$ [32]

$$\mathbf{F}_{k-1} = \mathbf{I}_3 \otimes \begin{bmatrix} 1 & T_0 \\ 0 & 1 \end{bmatrix} \tag{2}$$

$$\mathbf{Q}_{q,k-1} = \tau_q \mathbf{I}_3 \otimes \begin{bmatrix} {T_0}^3/3 & {T_0}^2/2 \\ {T_0}^2/2 & T_0 \end{bmatrix} \tag{3}$$

where $\mathbf{I}_3$ is the identity matrix of order 3, $\otimes$ is the Kronecker product, and τ_q denotes the process noise intensity [33].

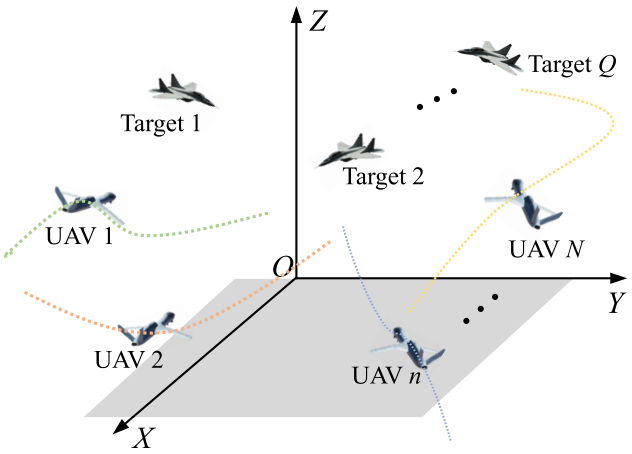

Fig. 1. Typical scenario where N UAVs track Q targets.

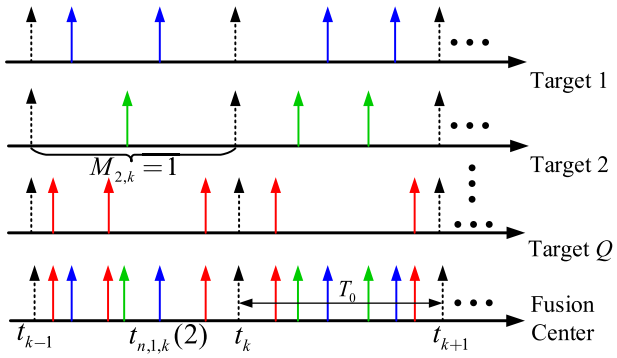

Fig. 2. Asynchronous measurements span fusion time intervals.

B. Dynamic Model for UAV n

As is shown in Fig. 1, we consider UAV n flies in 3-D Cartesian coordinates. Since the fusion time interval is small generally, the dynamic of UAV n can be described as a constant velocity model during the fusion time interval (t_{k-1}, t_k)

$$\mathbf{p}_{n,k} = \mathbf{p}_{n,k-1} + \mathbf{v}_{n,k}T_0, \ \ \mathbf{v}_{n,k} \in \mathbf{V}_{n,k} \tag{4}$$

where $\mathbf{V}_{n,k} = \{\mathbf{v}_{n,k} \mid \|\mathbf{v}_{n,k}\|_2 \le v_{\max}^n, \measuredangle(\mathbf{v}_{n,k}, \mathbf{v}_{n,k-1}) \le \alpha_{\max}^n\}$ implies the velocity of UAV n is restricted by the maximum speed $v_{\max}^n$ and the maximum turning angle $\alpha_{\max}^n$, and $\measuredangle(\mathbf{v}_{n,k}, \mathbf{v}_{n,k-1})$ denotes the angle formed by vectors $\mathbf{v}_{n,k}$ and $\mathbf{v}_{n,k-1}$. From (4), we see the position of UAV n at time t_k is decided by the velocity $\mathbf{v}_{n,k}$ for the given initial position $\mathbf{p}_{n,k-1}$. $\mathbf{v}_{n,k}$ can be adjusted at time t_{k-1} and maintain a constant during the fusion time interval (t_{k-1}, t_k). Limited by dynamic constraints, the possible positions of UAV n at time instant t_k are collected in the set $\mathbf{D}_{n,k}$, given by

$$\mathbf{D}_{n,k} = \{\mathbf{p}_{n,k} \mid \|\mathbf{p}_{n,k} - \mathbf{p}_{n,k-1}\|_2 \le v_{\max}^n T_0 \ \measuredangle\big((\mathbf{p}_{n,k} - \mathbf{p}_{n,k-1})/T_0, \mathbf{v}_{n,k-1}\big) \le \alpha_{\max}^n\}. \tag{5}$$

C. Measurement Model for Target q w.r.t. UAV n

During the kth fusion time interval (t_{k-1}, t_k), each sensor may receive multiple measurements from different targets, as shown in Fig. 2. We define $M_{n,q,k}$ as the number of

measurements received by sensor n from target q and refer to $t_{n,q,k}(m)$ as the arrival time of the mth measurement from target q w.r.t. sensor n. The number of measurements $M_{n,q,k}$ obeys a Poisson process with an exponential interarrival time [34]. It is assumed that the sensor network has been synchronized. In this case, the arrival time of AOA measurements for target q w.r.t. different sensors are the same, i.e., $t_{1,q,k}(m) = t_{2,q,k}(m) = \cdots = t_{N,q,k}(m) = t_{q,k}(m)$ and $M_{1,q,k} = M_{2,q,k} = \cdots = M_{N,q,k} = M_{q,k}$. The arrival time interval between two successive AOA measurements from target q received by sensor n may not be equal. During the kth fusion time interval, the mth AOA measurement from target q received by sensor n is

$$\mathbf{z}_{n,q,k}^{m} = \mathbf{h}(\mathbf{x}_{q,k}^{p}(m), \mathbf{p}_{n,k}(m)) + \mathbf{w}_{n,q,k}^{m} \tag{6}$$

where $\mathbf{h}(\mathbf{x}_{q,k}^{p}(m), \mathbf{p}_{n,k}(m))$ is the measurement function

$$\begin{aligned}\mathbf{h}\left(\mathbf{x}_{q,k}^{p}(m), \mathbf{p}_{n,k}(m)\right) &= \left[\theta_{n,q,k}^{m}, \varphi_{n,q,k}^{m}\right]^{T} \\ &= \begin{bmatrix} \arctan\left(\left(y_{q,k}^{m} - y_{n,k}^{m}\right)/\left(x_{q,k}^{m} - x_{n,k}^{m}\right)\right) \\ \arctan\left(d_{n,q,k}^{m}/\left(z_{q,k}^{m} - z_{n,k}^{m}\right)\right) \end{bmatrix}\end{aligned} \tag{7}$$

where $\mathbf{x}_{q,k}^{p}(m) = (x_{q,k}^{m}, y_{q,k}^{m}, z_{q,k}^{m})^{T}$ is the position of target q at time $t_{q,k}(m)$, $\mathbf{p}_{n,k}(m) = (x_{n,k}^{m}, y_{n,k}^{m}, z_{n,k}^{m})^{T}$ is the position of UAV n, $d_{n,q,k}^{m} = ((x_{q,k}^{m} - x_{n,k}^{m})^{2} + (y_{q,k}^{m} - y_{n,k}^{m})^{2})^{1/2}$ is the distance from the qth target to UAV n in xy plane, $\theta_{n,q,k}^{m} \in [0, 2\pi]$ and $\varphi_{n,q,k}^{m} \in [0, \pi]$ are azimuth and elevation, respectively. In (6), $\mathbf{w}_{n,q,k}^{m}$ is the measurement noise that follows a zero-mean Gaussian distribution with covariance $\Sigma_{n,q,k}^{m} = \text{blkdiag}(\sigma_{\theta_{n,q,k}^{m}}^{2}, \sigma_{\varphi_{n,q,k}^{m}}^{2})$, i.e., $\mathbf{w}_{n,q,k}^{m} \sim \mathcal{N}(\mathbf{0}, \Sigma_{n,q,k}^{m})$ [35]. The notation blkdiag$(\cdot)$ is a block diagonal operator, $\sigma_{\theta_{n,q,k}^{m}}^{2}$ and $\sigma_{\varphi_{n,q,k}^{m}}^{2}$ are CRLBs on ML estimates of azimuth $\theta_{n,q,k}^{m}$ and elevation $\varphi_{n,q,k}^{m}$, respectively [36]

$$\begin{cases} \sigma_{\theta_{n,q,k}^{m}}^{2} \propto \left(\kappa_{n,q,k}^{m}\theta_{3\,\text{dB}}^{-2}/\left(R_{n,q,k}^{m}\right)^{2}\right)^{-1} \\ \sigma_{\varphi_{n,q,k}^{m}}^{2} \propto \left(\kappa_{n,q,k}^{m}\varphi_{3\,\text{dB}}^{-2}/(R_{n,q,k}^{m})^{2}\right)^{-1} \end{cases} \tag{8}$$

where $\propto$ is a proportional operator, $\kappa_{n,q,k}^{m}$ is the radar cross section (RCS) of target q w.r.t. UAV n. $\theta_{3\,\text{dB}}$ and $\varphi_{3\,\text{dB}}$ are the 3 dB receive beamwidth in azimuth and elevation, respectively [36]. $R_{n,q,k}^{m} = \|\mathbf{x}_{q,k}^{p}(m) - \mathbf{p}_{n,k}(m)\|_{2}$ represents the distance from the qth target to the nth UAV. It can be observed that the measurement error will decrease as the UAV approaches the target.

III. MTT With Asynchronous Measurements

We assume that multiple targets are widely separated in the surveillance area. In this scenario, the MTT task can be divided into several independent single-target tracking problems. A two-step method is applied for target tracking with asynchronous AOA measurements. First, the ML method is employed to construct CMs for multiple targets at each fusion time instant [28]. Then, we adopt the KF for state estimation and prediction [37].

A. Formation of CM for Target q

The CM for target q at the fusion time instant t_k is $\bar{\mathbf{x}}_{q,k}$, which can be estimated by maximizing the likelihood function of $\mathbf{x}_{q,k}$, based on the AOA measurements span the fusion time interval (t_{k-1}, t_k)

$$\mathbf{Z}_{q,k} = \left[\mathbf{z}_{1,q,k}^{1T}, \ldots, \mathbf{z}_{N,q,k}^{1T}, \ldots, \mathbf{z}_{1,q,k}^{M_{q,k}T}, \ldots, \mathbf{z}_{N,q,k}^{M_{q,k}T}\right]^{T}. \tag{9}$$

The probability density function (pdf) of $\mathbf{Z}_{q,k}$ conditioned on $\mathbf{x}_{q,k}$ is $p\left(\mathbf{Z}_{q,k} \mid \mathbf{x}_{q,k}\right)$, then the ML estimator $\bar{\mathbf{x}}_{q,k}$ is

$$\begin{aligned}\bar{\mathbf{x}}_{q,k} &= \arg\max_{\mathbf{x}_{q,k}} \ln p\left(\mathbf{Z}_{q,k} \mid \mathbf{x}_{q,k}\right) \\ &= \arg\min_{\mathbf{x}_{q,k}} \Gamma\left(\mathbf{Z}_{q,k} \mid \mathbf{x}_{q,k}\right)\end{aligned} \tag{10}$$

where $\Gamma\left(\mathbf{Z}_{q,k} \mid \mathbf{x}_{q,k}\right)$ is

$$\begin{aligned}\Gamma(\mathbf{Z}_{q,k} \mid \mathbf{x}_{q,k}) = &\sum_{m=1}^{M_{q,k}} \sum_{n=1}^{N} \left(\mathbf{z}_{n,q,k}^{m} - \mathbf{h}\left(\mathbf{x}_{q,k}^{p}(m), \mathbf{p}_{n,k}(m)\right)\right)^{T} \\ &\times \left(\Sigma_{n,q,k}^{m}\right)^{-1} \left(\mathbf{z}_{n,q,k}^{m} - \mathbf{h}\left(\mathbf{x}_{q,k}^{p}(m), \mathbf{p}_{n,k}(m)\right)\right).\end{aligned} \tag{11}$$

From (10) and (11), we convert the ML problem as a weighted least square problem. It is hard for us to obtain a closed-form solution to problem (10) since $\Gamma\left(\mathbf{Z}_{q,k} \mid \mathbf{x}_{q,k}\right)$ is a nonlinear function. Consequently, the ML estimate can be obtained by the Newton iteration method [38], the state estimate for target q after the lth iteration is

$$\begin{aligned}\bar{\mathbf{x}}_{q,k}^{l+1} = \bar{\mathbf{x}}_{q,k}^{l} + &\left(\left(\mathbf{H}_{q,k}^{l}\right)^{T} \Sigma_{q,k}^{-1} \mathbf{H}_{q,k}^{l}\right)^{-1} \\ &\times \left(\mathbf{H}_{q,k}^{l}\right)^{T} \Sigma_{q,k}^{-1} \left(\mathbf{Z}_{q,k} - \mathbf{h}\left(\bar{\mathbf{x}}_{q,k}^{l}\right)\right)\end{aligned} \tag{12}$$

where the nonlinear measurement function can be represented as follows:

$$\mathbf{h}(\bar{\mathbf{x}}_{q,k}^{l}) = \begin{bmatrix} \mathbf{h}\left(\mathbf{F}(t_{q,k}(1), t_k)\bar{\mathbf{x}}_{q,k}^{l}, \mathbf{p}_{1,k}(1)\right) \\ \vdots \\ \mathbf{h}\left(\mathbf{F}(t_{q,k}(m), t_k)\bar{\mathbf{x}}_{q,k}^{l}, \mathbf{p}_{n,k}(m)\right) \\ \vdots \\ \mathbf{h}\left(\mathbf{F}(t_{q,k}(M_{q,k}), t_k)\bar{\mathbf{x}}_{q,k}^{l}, \mathbf{p}_{N,k}(M_{q,k})\right) \end{bmatrix}. \tag{13}$$

In (13), $\mathbf{h}\left(\mathbf{F}(t_{q,k}(m), t_k)\bar{\mathbf{x}}_{q,k}^{l}, \mathbf{p}_{n,k}(m)\right)$ predictes the measurement from the fusion time t_k to the arrival time $t_{q,k}(m)$, where $\mathbf{F}(t_{q,k}(m), t_k)$ denotes the transition matrix

$$\mathbf{F}(t_{q,k}(m), t_k) = \mathbf{I}_3 \otimes \begin{bmatrix} 1 & t_{q,k}(m) - t_k \\ 0 & 1 \end{bmatrix}. \tag{14}$$

In (12), $\Sigma_{q,k} = \text{blkdiag}(\Sigma_{1,q,k}^{1}, \ldots, \Sigma_{n,q,k}^{m}, \ldots, \Sigma_{N,q,k}^{M_{q,k}})$ denotes the covariance matrix of the measurement noise, $\mathbf{H}_{q,k}^{l}$ is the Jacobian matrix at the lth iteration

$$\begin{aligned}\mathbf{H}_{q,k}^{l} = [&\mathbf{H}_{1,q,k}^{lT}(1), \mathbf{H}_{2,q,k}^{lT}(1), \ldots, \\ &\mathbf{H}_{n,q,k}^{lT}(m), \ldots, \mathbf{H}_{N,q,k}^{lT}(M_{q,k})]^{T}\end{aligned} \tag{15}$$

where $\mathbf{H}^{l}_{n,q,k}(m)$ corresponding to the mth measurement evaluated at $\bar{\mathbf{x}}^{l}_{q,k}$

$$\mathbf{H}^{l}_{n,q,k}(m) = \nabla_{\mathbf{x}^{l^T}_{q,k}(m)} \mathbf{h}\left(\mathbf{x}^{l}_{q,k}(m), \mathbf{p}_{n,k}(m)\right) \times \mathbf{F}(t_{q,k}(m), t_k) \tag{16}$$

where ∇ denotes the partial derivative operator, and $\mathbf{x}^{l}_{q,k}(m) = \mathbf{F}(t_{q,k}(m), t_k)\bar{\mathbf{x}}^{l}_{q,k}$ predicts the target state from the fusion time t_k to the arrival time $t_{q,k}(m)$. An initial state estimate for the qth target is required for the Newton iteration method, which can take the predicted state, since the fusion time interval is small generally, e.g., two seconds as considered in this work.

The CRLB provides a lower bound for any unbiased estimator. Given the true state $\mathbf{x}_{q,k}$ and the state estimate $\bar{\mathbf{x}}_{q,k}$, the CRLB can be represented as

$$E\left[(\mathbf{x}_{q,k} - \bar{\mathbf{x}}_{q,k})(\mathbf{x}_{q,k} - \bar{\mathbf{x}}_{q,k})^T\right] \geq \mathbf{CB}^{-1}_{q,k} \tag{17}$$

where $\mathbf{CB}_{q,k}$ is the Fisher information matrix (FIM)

$$\mathbf{CB}_{q,k} \approx \mathbf{H}^{T}_{q,k} \Sigma^{-1}_{q,k} \mathbf{H}_{q,k} \mid_{\bar{\mathbf{x}}_{q,k}} . \tag{18}$$

The FIM requires knowledge of the true state of the target, which is unknown in practice. Therefore, the FIM is approximated by replacing the true state with the CM produced by the ML estimator. It is shown that the ML estimator is statistically efficient for as few as two AOA measurements [28] (variety with UAV−target geometries). Therefore, the CRLB matrix can be used as the measurement-noise covariance for the resulting CM $\bar{\mathbf{x}}_{q,k}$ in the KF.

B. The KF for Target q

Suppose that the track initialization is available, and thus, we can obtain the initial state estimate $\hat{\mathbf{x}}_{q,k=0}$ and the corresponding initial covariance $\hat{\mathbf{P}}_{q,k=0}$ for target q. It is assumed that the pdf of $\mathbf{x}_{q,k}$ follows a Gaussian distribution, i.e., $p(\mathbf{x}_{q,k}|\bar{\mathbf{x}}_{q,k}) = \mathcal{N}(\hat{\mathbf{x}}_{q,k}, \hat{\mathbf{P}}_{q,k})$, where $\hat{\mathbf{x}}_{q,k}$ and $\hat{\mathbf{P}}_{q,k}$ are the state estimate and the corresponding covariance, respectively. From (1), the predicted pdf is $p(\mathbf{x}_{q,k}|\bar{\mathbf{x}}_{q,k-1}) = \mathcal{N}(\mathbf{x}_{q,k|k-1}, \mathbf{P}_{q,k|k-1})$, and the predicted state $\mathbf{x}_{q,k|k-1}$ and corresponding covariance $\mathbf{P}_{q,k|k-1}$ are [37]

$$\mathbf{x}_{q,k|k-1} = \mathbf{F}_{k-1}\hat{\mathbf{x}}_{q,k-1} \tag{19}$$

$$\mathbf{P}_{q,k|k-1} = \mathbf{F}_{k-1}\hat{\mathbf{P}}_{q,k-1}\mathbf{F}^{T}_{k-1} + \mathbf{Q}_{q,k-1}. \tag{20}$$

If no measurements are received from the qth target during the kth fusion time interval, the KF regards the predicted state and the corresponding covariance as the state estimate and the estimated covariance, respectively. On the contrary, the innovation and the corresponding covariance can be obtained from the predicted state and the CM as

$$\boldsymbol{\vartheta}_{q,k} = \bar{\mathbf{x}}_{q,k} - \mathbf{x}_{q,k|k-1} \tag{21}$$

$$\mathbf{S}_{q,k} = \mathbf{P}_{q,k|k-1} + \mathbf{CB}^{-1}_{q,k}. \tag{22}$$

In (21), $\mathbf{x}_{q,k|k-1} = \mathbf{F}_{k-1}\hat{\mathbf{x}}_{q,k-1}$ is the predicted state. The state estimate $\hat{\mathbf{x}}_{q,k}$ and the corresponding covariance $\hat{\mathbf{P}}_{q,k}$ can be obtained by

$$\hat{\mathbf{x}}_{q,k} = \mathbf{x}_{q,k|k-1} + \mathbf{G}_{q,k}\boldsymbol{\vartheta}_{q,k} \tag{23}$$

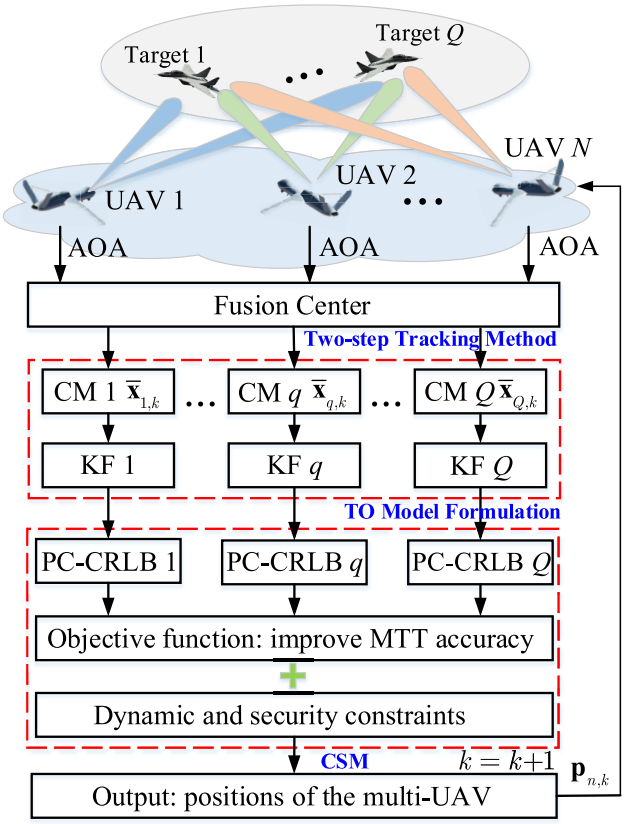

Fig. 3. Closed-loop asynchronous tracking framework for CTO.

$$\hat{\mathbf{P}}_{q,k} = \mathbf{P}_{q,k|k-1} - \mathbf{G}_{q,k}\mathbf{P}_{q,k|k-1} \tag{24}$$

where $\mathbf{G}_{q,k} = \mathbf{P}_{q,k|k-1}\mathbf{S}^{-1}_{q,k}$ is the Kalman gain [37].

IV. CTO for Passive MTT

This article aims to collaboratively optimize the trajectories of multi-UAV to maximize the MTT performance. The closed-loop asynchronous tracking framework is shown in Fig. 3, where the two-step tracking method is utilized for state estimation and prediction. According to the prediction information, the PC-CRLB of each target can be calculated, then the summation of these PC-CRLBs is used as the objective function of the CTO problem. The dynamic and security constraints can be specified according to the UAV's performance parameters and application scenarios. Finally, the CSM is proposed for the resulting CTO problem to guide the waypoints of multi-UAV next time. We first formulate the CTO model and then introduce the CSM.

A. PC-CRLB for Target q

The PC-CRLB is adopted as the tracking performance measure to predetermine the waypoints of multi-UAV at the next fusion time, which is defined as [30]

$$E_{\mathbf{x}_{q,k},\mathbf{Z}_{q,k}|\mathbf{Z}_{q,1:k-1}}\left\{\left[\hat{\mathbf{x}}_{q,k} - \mathbf{x}_{q,k}\right]\left[\hat{\mathbf{x}}_{q,k} - \mathbf{x}_{q,k}\right]^T\right\} \geq \mathbf{J}^{-1}\left(\mathbf{x}_{q,k}|\mathbf{Z}_{q,1:k-1}\right) \tag{25}$$

where $\mathbf{J}(\mathbf{x}_{q,k})$ is the predicted conditional FIM (PC-FIM), whose inverse is the PC-CRLB. The PC-FIM is

$$\mathbf{J}\left(\mathbf{x}_{q,k}|\mathbf{Z}_{q,1:k-1}\right) = E_{\mathbf{x}_{q,k},\mathbf{Z}_{q,k}|\mathbf{Z}_{q,1:k-1}} \times \left\{-\Delta_{\mathbf{x}_{q,k}}^{\mathbf{x}_{q,k}} \log p\left(\mathbf{x}_{q,k}, \mathbf{Z}_{q,k}|\mathbf{Z}_{q,1:k-1}\right)\right\}. \tag{26}$$

In (26), $p\left(\mathbf{x}_{q,k}, \mathbf{Z}_{q,k}|\mathbf{Z}_{q,1:k-1}\right)$ is the joint pdf conditioned on the set $\mathbf{Z}_{q,1:k-1}$ that collects measurements from time t_1 to t_{k-1}, and $\Delta_{\mathbf{x}_{q,k}}^{\mathbf{x}_{q,k}}$ denotes a second-order partial derivative operator w.r.t. $\mathbf{x}_{q,k}$. The PC-FIM can be simplified as the summation of two terms as follows:

$$\mathbf{J}\left(\mathbf{x}_{q,k}|\mathbf{Z}_{q,1:k-1}\right) = \mathbf{J}_P\left(\mathbf{x}_{q,k}|\mathbf{Z}_{q,1:k-1}\right) + \mathbf{J}_D\left(\mathbf{x}_{q,k}|\mathbf{Z}_{q,1:k-1}\right). \tag{27}$$

In (27), $\mathbf{J}_P(\mathbf{x}_{q,k}|\mathbf{Z}_{q,1:k-1})$ is the prior information term

$$\mathbf{J}_P\left(\mathbf{x}_{q,k}|\mathbf{Z}_{q,1:k-1}\right) = E_{\mathbf{x}_{q,k}|\mathbf{Z}_{q,1:k-1}}\left\{-\Delta_{\mathbf{x}_{q,k}}^{\mathbf{x}_{q,k}} \log p\left(\mathbf{x}_{q,k}|\mathbf{Z}_{q,1:k-1}\right)\right\} \tag{28}$$

where the expectation is taken w.r.t. the predicted pdf. It is hard to analytically evaluate the $\mathbf{J}_P\left(\mathbf{x}_{q,k}|\mathbf{Z}_{q,1:k-1}\right)$. Since the predicted pdf of the target q obeys a Gaussian distribution, we can approximate $\mathbf{J}_P\left(\mathbf{x}_{q,k}|\mathbf{Z}_{q,1:k-1}\right)$ as the inverse of the predicted covariance matrix, i.e., $\mathbf{J}_P\left(\mathbf{x}_{q,k}|\mathbf{Z}_{q,1:k-1}\right) \approx \mathbf{P}_{k|k-1}^{-1}$.

In (27), $\mathbf{J}_D\left(\mathbf{x}_{q,k}|\mathbf{Z}_{q,1:k-1}\right)$ is the data information term, which can be expressed as follows:

$$\mathbf{J}_D\left(\mathbf{x}_{q,k}\,|\,\mathbf{Z}_{q,1:k-1}\right) = E_{\mathbf{x}_{q,k},\mathbf{Z}_{q,k}|\mathbf{Z}_{q,1:k-1}}\left\{-\Delta_{\mathbf{x}_{q,k}}^{\mathbf{x}_{q,k}} \log p\left(\mathbf{Z}_{q,k}\,|\,\mathbf{x}_{q,k}\right)\right\} \tag{29}$$

Similarly, the evaluation of $\mathbf{J}_D(\mathbf{x}_{q,k}|\mathbf{Z}_{q,1:k-1})$ involves the expectation operation, which is usually implemented by the Monte Carlo experiments. Under the assumption that the process noise is relatively small, we can approximate $\mathbf{J}_D(\mathbf{x}_{q,k}|\mathbf{Z}_{q,1:k-1})$ as [39]

$$\mathbf{J}_D\left(\mathbf{x}_{q,k}|\mathbf{Z}_{q,1:k-1}\right) \approx \sum_{n=1}^{N} \bar{\mathbf{H}}_{n,q,k}^T(\mathbf{p}_{n,k})\Sigma_{n,q,k}^{-1}(\mathbf{p}_{n,k})\bar{\mathbf{H}}_{n,q,k}(\mathbf{p}_{n,k})\,|_{\mathbf{x}_{q,k|k-1}}. \tag{30}$$

The arrival time of measurements w.r.t. target q span randomly in the fusion time interval (t_{k-1}, t_k), and we cannot predict them at the time instant t_{k-1}. Therefore, we calculate $\mathbf{J}_D(\mathbf{x}_{q,k}|\mathbf{Z}_{q,1:k-1})$ according to the predicted state from the fusion time instant t_{k-1} to t_k. In (30), $\Sigma_{n,q,k}(\mathbf{p}_{n,k})$ is the predicted covariance of the measurement noise [see (8) for details]. $\bar{\mathbf{H}}_{n,q,k}(\mathbf{p}_{n,k})$ means that the predicted Jacobian matrix is a function of the UAV's position

$$\bar{\mathbf{H}}_{n,q,k}(\mathbf{p}_{n,k}) = \nabla_{\mathbf{x}_{q,k|k-1}^T}\mathbf{h}\left(\mathbf{x}_{q,k|k-1}, \mathbf{p}_{n,k}\right) = \begin{bmatrix} \frac{\partial\theta_{q,k}}{\partial x_{q,k}} & 0 & \frac{\partial\theta_{q,k}}{\partial y_{q,k}} & 0 & 0 & 0 \\ \frac{\partial\varphi_{q,k}}{\partial x_{q,k}} & 0 & \frac{\partial\varphi_{q,k}}{\partial y_{q,k}} & 0 & \frac{\partial\varphi_{q,k}}{\partial z_{q,k}} & 0 \end{bmatrix} \tag{31}$$

where components of the partial derivatives are

$$\begin{aligned} \frac{\partial\theta_{q,k}}{\partial x_{q,k}} &= -\frac{y_{q,k|k-1} - y_{n,k}}{d_{n,q,k|k-1}}, \quad \frac{\partial\theta_{q,k}}{\partial y_{q,k}} = \frac{x_{q,k|k-1} - x_{n,k}}{d_{n,q,k|k-1}} \\ \frac{\partial\varphi_{q,k}}{\partial x_{q,k}} &= \frac{(x_{q,k|k-1} - x_{n,k})(z_{q,k|k-1} - z_{n,k})}{d_{n,q,k|k-1}R_{n,q,k|k-1}^2} \\ \frac{\partial\varphi_{q,k}}{\partial y_{q,k}} &= \frac{(y_{q,k|k-1} - y_{n,k})(z_{q,k|k-1} - z_{n,k})}{d_{n,q,k|k-1}R_{n,q,k|k-1}^2} \\ \frac{\partial\varphi_{q,k}}{\partial z_{q,k}} &= -\frac{d_{n,q,k|k-1}}{R_{n,q,k|k-1}^2}. \end{aligned} \tag{32}$$

In (32), $R_{n,q,k|k-1} = \|\mathbf{p}_{n,k} - \mathbf{x}_{q,k|k-1}^p\|_2$ is the predicted distance from UAV n to target q, $d_{n,q,k|k-1} = ((\mathbf{x}_{q,k|k-1} - \mathbf{x}_{n,k})^2 + (\mathbf{y}_{q,k|k-1} - \mathbf{y}_{n,k})^2)^{1/2}$ denotes the predicted distance in xy plane.

Based on the above-mentioned derivation, we can rewrite the PC-FIM as follows:

$$\mathbf{J}\left(\mathbf{x}_{q,k}|\mathbf{Z}_{q,1:k-1}\right) = \mathbf{P}_{q,k|k-1}^{-1} + \sum_{n=1}^{N} \bar{\mathbf{H}}_{n,q,k}^T(\mathbf{p}_{n,k})\Sigma_{n,q,k}^{-1} \times (\mathbf{p}_{n,k})\bar{\mathbf{H}}_{n,q,k}(\mathbf{p}_{n,k})\,|_{\mathbf{x}_{q,k|k-1}}. \tag{33}$$

B. CTO Model

The PC-FIM (33) shows that the positions of multi-UAV have an impact on the tracking performance, which motivates us to optimize the trajectories of multiple UAVs to achieve the optimal MTT performance. Since the elements of the PC-CRLB matrix have different units, it cannot be adopted as an objective function directly, we perform a trace operation on the normalized PC-CRLB as follows:

$$f_q(\mathbf{p}_k) = \mathrm{Tr}\left(\mathbf{\Lambda}^T\mathbf{J}^{-1}\left(\mathbf{x}_{q,k}|\mathbf{Z}_{q,1:k-1}\right)\mathbf{\Lambda}\right) \tag{34}$$

where the position vector of multi-UAV is defined as $\mathbf{p}_k = (\mathbf{p}_{1,k}^T, \mathbf{p}_{2,k}^T, \ldots, \mathbf{p}_{N,k}^T)^T$, and $\mathbf{\Lambda} = \mathbf{I}_3 \otimes \mathrm{blkdiag}(1, T_0)$ is the normalization matrix.

In general, the trajectories of UAVs are subject to some dynamic and security constraints. The dynamic constraints are given in (5), the first type of security constraint is that the flying altitude of each UAV should be greater than or equal to the minimum height $H_{\min}$

$$\mathbf{p}_{n,k}(3) \geq H_{\min}, \quad n \in \mathbf{\Omega}_{a,k} \tag{35}$$

where $\mathbf{p}_{n,k}(3)$ denotes the third element of $\mathbf{p}_{n,k}$, and $\mathbf{\Omega}_{a,k}$ is a set that collects all indexes of UAVs that may fly below the minimum height at the next time step.

The second type of security constraint is that any two UAVs should be separated by a certain distance d_{col}, that is, for all $(n_1, n_2) \in \mathbf{\Omega}_{s,k}$ and $n_2 > n_1$

$$\|\mathbf{p}_{n_1,k} - \mathbf{p}_{n_2,k}\|_2 \geq d_{\mathrm{col}}, \quad (n_1, n_2) \in \mathbf{\Omega}_{s,k} \tag{36}$$

where $\mathbf{\Omega}_{s,k}$ is a set that collects all index pairs of any two UAVs which may collide. In other words, if two UAVs are unlikely to appear in their respective range of motion during the next fusion time interval, the constraint (36) will not work.

The third kind of security constraint is that each UAV should keep a minimum clearance distance r_i from a given position $\mathbf{c}_i$, that is, for all $(n, i) \in \mathbf{\Omega}_{b,k}$

$$\|\mathbf{p}_{n,k} - \mathbf{c}_{i,k}\|_2 \geq r_i, \ \ (n, i) \in \mathbf{\Omega}_{b,k}. \tag{37}$$

These constraints (37) can be configured to achieve obstacle/target/threat avoidance by appropriately selecting $\mathbf{c}_{i,k}$ and r_i, $i \in \{1, 2, \ldots, N_B + N_T + Q\}$, where N_B and N_T denote the number of obstacle points and threats, respectively. The obstacle points are given by a 3-D digital terrain map [40], which is reloaded at each fusion time instant. The positions of threats (e.g., enemy radars) are assumed known. If $\mathbf{c}_{i,k} = \mathbf{x}^p_{q,k|k-1}$, it means that the UAV should keep a distance from target q to avoid being detected by it. Similarly, if the UAV n is far away from the obstacle i, i.e., $(n, i) \notin \mathbf{\Omega}_{b,k}$, this constraint will be inactive. The constraints (37) may also be modified to define arbitrary noncircular no-fly zones.

Combining (5) and (IV-B)–(37), we formulate the time-varying CTO model as

$$\min_{\mathbf{p}_k} \ f(\mathbf{p}_k)$$
$$\text{s.t.} \begin{cases} \mathbf{p}_{n,k} \in \mathbf{D}_{n,k}, \ \ n = 1, 2, \ldots, N \\ \mathbf{p}_{n,k}(3) \geq H_{\min}, \ \ n \in \mathbf{\Omega}_{a,k} \\ \|\mathbf{p}_{n,k} - \mathbf{c}_{i,k}\|_2 \geq r_i, \ \ (n, i) \in \mathbf{\Omega}_{s,k} \\ \|\mathbf{p}_{n_1,k} - \mathbf{p}_{n_2,k}\|_2 \geq d_{\text{col}}, \ \ (n_1, n_2) \in \mathbf{\Omega}_{b,k} \end{cases} \tag{38}$$

where $f(\mathbf{p}_k) = \sum_{q=1}^{Q} f_q(\mathbf{p}_k)$ denotes the overall MTT accuracy. Note that the security constraints (36) and (37) are nonconvex sets and the objective is a nonconvex function, and the CTO model (38) is a time-varying nonconvex optimization problem, which is hard to obtain its optimal solution. In the following, the CSM is proposed to find the suboptimal trajectories of multiple UAVs in different situations.

The following remarks may be deduced from the CTO model (38).

Remark 1: We note that the minimum flying height constraint in (38) may be redundant when specific obstacle avoidance constraints are enforced. For instance, the height constraint becomes redundant when clearance distances for obstacle point avoidance are much larger than the minimum flying height, i.e., $r_i \gg H_{\min}$. On the other hand, if UAVs are far from obstacle points and require keeping high-altitude flying, then the minimum flying height constraint is necessary.

Remark 2: In [10], [11], [12], [13], [14], the heading angle and speed are adopted as optimization variables, and the dynamic model for UAV n is reformulated as $\mathbf{p}_{n,k} = \mathbf{p}_{n,k-1} + v_{n,k} T_0 \boldsymbol{\varsigma}_{n,k}$, where $v_{n,k} \leq v^n_{\max}$ is the speed of UAV n, $\boldsymbol{\varsigma}_{n,k} = [\cos(\beta_{n,k})\cos(\phi_{n,k}), \sin(\beta_{n,k})\cos(\phi_{n,k}), \sin(\phi_{n,k})]^T$ is the direction vector of velocity. $\beta_{n,k}$ and $\phi_{n,k}$ are azimuth and elevation of the velocity, respectively, which satisfies $\measuredangle(\boldsymbol{\varsigma}_{n,k}, \boldsymbol{\varsigma}_{n,k-1}) \leq \alpha^n_{\max}$. The adaptable variables in the new dynamic model are $\{v_{n,k}, \beta_{n,k}, \phi_{n,k}\}$. We see that the new formulation is equivalent to model (4), but it introduces transcendental functions, which increases the nonlinearity of security constraints. Therefore, the dynamic and CTO models we built are simpler than the previous studies [10], [11], [12], [13], [14].

Algorithm 1 The NSPG Method

Input: $l = 0$, λ^l_k, $\mathbf{p}^l_k$, ε, $\lambda_{\min}$ and $\lambda_{\max}$;
repeat
1. Calculate the search direction:
$\mathbf{d}^l_k = \mathcal{P}_{\mathbf{D}_k}(\mathbf{p}^l_k - \lambda^l_k \nabla_{\mathbf{p}^l_k} f(\mathbf{p}_k)) - \mathbf{p}^l_k$;
2. Calculate the step length γ^l_k according to Algorithm 2 and set $\mathbf{p}^{l+1}_k = \mathbf{p}^l_k + \gamma^l_k \mathbf{d}^l_k$
3. Update the spectral step length:
Let $\mathbf{p}'^l_k = \mathbf{p}^{l+1}_k - \mathbf{p}^l_k$ and
$\mathbf{y}^l_k = \nabla_{\mathbf{p}^{l+1}_k} f(\mathbf{p}_k) - \nabla_{\mathbf{p}^l_k} f(\mathbf{p}_k)$
if $\mathbf{p}'^{lT}_k \mathbf{y}^l_k \leq 0$ **then**
$\lambda^{l+1}_k = \lambda_{\max}$;
else
$\lambda^{l+1}_k = \max\{\lambda_{\min}, \min\{\lambda_{\max}, \mathbf{p}'^{lT}_k \mathbf{p}'^l_k / \mathbf{p}'^{lT}_k \mathbf{y}^l_k\}\}$;
end
4. Let $l = l + 1$;
until $\|\mathcal{P}_{\mathbf{D}_k}(\mathbf{p}^l_k - \nabla_{\mathbf{p}^l_k} f(\mathbf{p}_k)) - \mathbf{p}^l_k\|_\infty \leq \varepsilon$;
Return: $\mathbf{p}_k = \mathbf{p}^l_k$.

C. CSM for the CTO Problem

In this section, the CSM is designed to solve the nonconvex problem (37) by exploring its time-varying property. The CSM begins with a judgment of which security constraints are active based on the current position and velocity of the UAV as well as the target. According to whether the security constraints work, we design two algorithms to obtain the suboptimal trajectories of multi-UAV. Then, the CSM is presented based on the two algorithms.

Case 1 (CTO Without Security Constraints): If any two UAVs are far apart at an altitude higher than $H_{\min}$, and the UAVs are far away from multiple targets, threats, and obstacles, the security constraints may not work. In this case, the CTO model can be recast as

$$\min_{\mathbf{p}_k} \ f(\mathbf{p}_k)$$
$$\text{s.t.} \ \ \mathbf{p}_{n,k} \in \mathbf{D}_{n,k}, \ \ n = 1, 2, \ldots, N \tag{39}$$

which is a nonconvex optimization problem with convex constraints, since $\mathbf{D}_{n,k}$ is the intersection of a ball and a cone. The PG method [10] can be applied to solve problem (39) for a suboptimal solution, but with a slow convergence rate. To this end, we introduce the spectral gradient idea with a nonmonotone line search (NLS) to the PG method to speed up its convergence [31]. The NSPG for problem (39) is given in **Algorithm 1**, where ε is the tolerance for the NSPG method, λ^l_k denotes the spectral step length at the lth iteration, $[\lambda_{\min}, \lambda_{\max}]$ are the minimum and maximum safeguarding parameters for λ^l_k, $\mathbf{D}_k = \mathbf{D}_{1,k} \cup \mathbf{D}_{2,k} \cup \cdots \cup \mathbf{D}_{N,k}$, and γ^l_k represents the step length that can be obtained by the NLS as listed in **Algorithm 2**.

In **Algorithm 2**, $\delta \in (0, 1)$ denotes a sufficient decrease parameter, L is an integer, and σ_1 and σ_2 are safeguarding

Algorithm 2 The NLS Method

Input: $\mathbf{d}_k^l$, $\mathbf{p}_k^l$, L, $\gamma_k^l = 1$, δ, σ_1 and σ_2;
Output: γ_k^l
repeat
1. Calculate $f_{\max} = \max_{0\le i\le \min\{l,L-1\}} f(\mathbf{p}_k^{l-i})$
2. Update the step length:
Calculate $\gamma_{temp} = -\frac{1}{2}\gamma_k^{l2}\nabla_{\mathbf{p}_k^l} f(\mathbf{p}_k)^T \mathbf{d}_k^l / \triangle f$,
$\triangle f = f(\mathbf{p}_k^l + \gamma_k^l \mathbf{d}_k^l) - f(\mathbf{p}_k^l) - \gamma_k^l \nabla_{\mathbf{p}_k^l} f(\mathbf{p}_k)^T \mathbf{d}_k^l$
if $\gamma_{temp} \in [\sigma_1, \sigma_2 \gamma_k^l]$ **then**
$\gamma_k^l = \gamma_{temp}$;
else
$\gamma_k^l = \gamma_k^l/2$;
end
until $f(\mathbf{p}_k^l + \gamma_k^l \mathbf{d}_k^l) - f_{\max} - \delta\gamma_k^l \nabla_{\mathbf{p}_k^l} f(\mathbf{p}_k)^T \mathbf{d}_k^l > 0$;

parameters that satisfy $0 < \sigma_1 < \sigma_2 < 1$. The main idea behind the NLS is that the steepest descent method is very slow but it can be accelerated by taking a step size that comes from the 1-D minimization at the previous step, instead of the one that comes from the minimization of the function along the gradient of the current iteration.

In **Algorithm 1**, $\mathcal{P}_{\mathbf{D}_k}(\mathbf{p}_k^{\text{temp}})$ represents an operator that projects the point $\mathbf{p}_k^{\text{temp}}$ to the feasible sets, which corresponds to the solution of problem (40)

$$\begin{aligned} &\min_{\mathbf{p}_k} \ \|\mathbf{p}_k - \mathbf{p}_k^{\text{temp}}\|_2 \\ &\text{s.t.} \quad \mathbf{p}_{n,k} \in \mathbf{D}_{n,k}, \ n = 1, 2, \ldots, N \end{aligned} \tag{40}$$

which can be easily solved by the interior point solver [41] but with a slow convergence rate and poor scalability. Instead, we propose a projection operator with a closed-form solution, which can be implemented parallelly. In particular, we can separate problem (40) into N subproblems, as the feasible domains of any two UAVs ($n_1 \neq n_2$) satisfy $\mathbf{D}_{n1,k} \cap \mathbf{D}_{n2,k} = \varnothing$, the nth subproblem is

$$\begin{aligned} &\min_{\mathbf{p}_{n,k}} \ \|\mathbf{p}_{n,k} - \mathbf{p}_{n,k}^{\text{temp}}\|_2 \\ &\text{s.t.} \quad \mathbf{p}_{n,k} \in \mathbf{D}_{n,k}. \end{aligned} \tag{41}$$

The optimal solution for problem (41) is $\mathcal{P}_{\mathbf{D}_{n,k}}(\mathbf{p}_{n,k}^{\text{temp}})$. The projection process for the given point $\mathbf{p}_{n,k}^{\text{temp}}$ involves the coordinate system transformation, as shown in Fig. 4. We first pan the origin coordinate system to the point $\mathbf{p}_{n,k-1}$, and then rotate the z-axis to the $\mathbf{v}_{n,k-1}$ direction. The rotation step includes rotating $\beta_{n,k-1}$ degrees around the z-axis and $\phi_{n,k-1}$ degrees around the y-axis. The rotation matrix is defined as $\mathbf{R}_{ot} = \mathbf{R}_{ot}^y \mathbf{R}_{ot}^z$, where

$$\mathbf{R}_{ot}^y = \begin{bmatrix} \cos(\phi_{n,k-1}) & 0 & -\sin(\phi_{n,k-1}) \\ 0 & 1 & 0 \\ \sin(\phi_{n,k-1}) & 0 & \cos(\phi_{n,k-1}) \end{bmatrix} \tag{42}$$

and

$$\mathbf{R}_{ot}^z = \begin{bmatrix} \cos(\beta_{n,k-1}) & \sin(\beta_{n,k-1}) & 0 \\ -\sin(\beta_{n,k-1}) & \cos(\beta_{n,k-1}) & 0 \\ 0 & 0 & 1 \end{bmatrix} \tag{43}$$

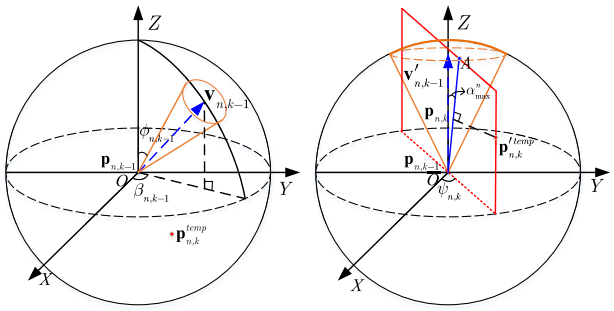

Fig. 4. Coordinate system transformation.

are rotation matrices w.r.t. y-axis and z-axis, respectively.

After coordinate transformation, the position of $\mathbf{p}_{n,k}^{\text{temp}}$ is given by

$$\mathbf{p}'^{\text{temp}}_{n,k} = \mathbf{R}_{ot}\left(\mathbf{p}_{n,k}^{\text{temp}} - \mathbf{p}_{n,k-1}\right). \tag{44}$$

Recalling that the feasible domain $\mathbf{D}_{n,k}$ is the intersection of a ball and a cone. We define OA (the generatrix of the cone in Fig. 4) to be the line segment where the point $\mathbf{p}'^{\text{temp}}_{n,k}$ lies, the coordinate of point A is

$$\begin{aligned} \mathbf{p}_{n,k}^A = & v_{\max}^n T_0 \big[\sin\left(\alpha_{\max}^n\right)\cos(\psi_{n,k}), \\ & \sin\left(\alpha_{\max}^n\right)\sin(\psi_{n,k}), \cos\left(\alpha_{\max}^n\right)\big]^T \end{aligned} \tag{45}$$

where $\psi_{n,k}$ is the azimuth of the point $\mathbf{p}'^{\text{temp}}_{n,k}$.

Then, the projected position of $\mathbf{p}_{n,k}^{\text{temp}}$ is

$$\mathbf{p}_{n,k}^{pro} = \max(0, \min(\eta_{n,k}, 1))\mathbf{p}_{n,k}^A \tag{46}$$

where $\eta_{n,k} = (\mathbf{p}_{n,k}^A)^T \mathbf{p}'^{\text{temp}}_{n,k} / \|\mathbf{p}_{n,k}^A\|_2$.

According to (44)–(46), we can obtain a closed-form expression for the projected point.

Case 2 (CTO With Security Constraints): In this case, some security constraints may be active during the tracking process, assuming that all three kinds of security constraints are activated, i.e., $\mathbf{\Omega}_{a,k}$, $\mathbf{\Omega}_{s,k}$, and $\mathbf{\Omega}_{b,k}$ are nonempty sets in problem (38). Note (38) is hard to deal with, since it may entail a number of coupled nonconvex constraints. In light of the challenge of computation, it is desirable to develop an efficient algorithm to obtain high-quality suboptimal solutions to problem (38). To this end, an ADPM is developed to solve it with guarantee convergence under several conditions.

To present the ADPM, we first define

$$a_{n,k} = \mathbf{p}_{n,k}(3), \ n \in \mathbf{\Omega}_{a,k} \tag{47}$$

and denote $\mathbf{a}_k$ as a vector concatenating all $a_{n,k}, n \in \mathbf{\Omega}_{a,k}$.

Based on (47), we can compactly rewrite (35) as

$$\mathbf{A}_1 \mathbf{p}_k = \mathbf{a}_k \tag{48}$$

where $\mathbf{A}_1$ is a coefficient matrix, which can be obtained from (47), the feasible domain of $\mathbf{a}_k$ is $\mathbf{D}_{a,k} = \{a_{n,k} \mid a_{n,k} \geq H_{\min}, n \in \mathbf{\Omega}_{a,k}\}$.

For the second type of security constraint, we define

$$\mathbf{s}_{n_{1,2},k} = \mathbf{p}_{n1,k} - \mathbf{p}_{n2,k}, \ (n1, n2) \in \mathbf{\Omega}_{s,k} \tag{49}$$

and let $\mathbf{s}_k$ be a vector that concatenates all the $\mathbf{s}_{n_{1,2},k}$, $(n1, n2) \in \mathbf{\Omega}_{s,k}$. A compact form of (49) is

$$\mathbf{A}_2\mathbf{p}_k = \mathbf{s}_k \tag{50}$$

where $\mathbf{A}_2$ is a coefficient matrix, which can be obtained from (49). From (36), the feasible domain of $\mathbf{s}_k$ is $\mathbf{D}_{s,k} = \{\mathbf{s}_{n_{1,2},k} \mid \|\mathbf{s}_{n_{1,2},k}\|_2 \geq d_{\text{col}},\ (n1, n2) \in \mathbf{\Omega}_{s,k}\}$.

Similarly, we define

$$\mathbf{b}_{ni,k} = \mathbf{p}_{n,k} - \mathbf{c}_{i,k},\ (n, i) \in \mathbf{\Omega}_{b,k} \tag{51}$$

where $\mathbf{b}_k$ is a vector that concatenates all the $\mathbf{b}_{ni,k}$, $(n, i) \in \mathbf{\Omega}_{b,k}$ with the feasible domain $\mathbf{D}_{b,k} = \{\mathbf{b}_{ni,k} \mid \|\mathbf{b}_{ni,k}\|_2 \geq r_i,\ (n, i) \in \mathbf{\Omega}_{b,k}\}$. Then, we can equivalently rewrite (37) as an equality constraint as

$$\mathbf{A}_3\mathbf{p}_k - \mathbf{c}_k = \mathbf{b}_k \tag{52}$$

where $\mathbf{A}_3$ is a coefficient matrix, and $\mathbf{c}_k$ is a vector that concatenates all the $\mathbf{c}_{i,k}$, $(\cdot, i) \in \mathbf{\Omega}_{b,k}$.

Then, we can equivalently reformulate (38) as

$$\min_{\mathbf{p}_k}\ f(\mathbf{p}_k) \quad \text{s.t.} \begin{cases} \mathbf{A}_1\mathbf{p}_k = \mathbf{a}_k \\ \mathbf{A}_2\mathbf{p}_k = \mathbf{s}_k \\ \mathbf{A}_3\mathbf{p}_k - \mathbf{c}_k = \mathbf{b}_k \\ \mathbf{a}_k \in \mathbf{D}_{a,k},\ \mathbf{s}_k \in \mathbf{D}_{s,k} \\ \mathbf{b}_k \in \mathbf{D}_{b,k},\ \mathbf{p}_{n,k} \in \mathbf{D}_{n,k}, \forall n. \end{cases} \tag{53}$$

The scaled augmented Lagrangian function of (53) is

$$\begin{aligned} &\mathcal{L}_\rho(\mathbf{p}_k, \mathbf{a}_k, \mathbf{s}_k, \mathbf{b}_k; \boldsymbol{\chi}_k, \boldsymbol{\mu}_k, \boldsymbol{\nu}_k, \rho_1, \rho_2, \rho_3) \\ &\quad = f(\mathbf{p}_k) + \frac{\rho_1}{2}\|\mathbf{A}_1\mathbf{p}_k - \mathbf{a}_k + \boldsymbol{\chi}_k\|_2^2 - \frac{\rho_1}{2}\|\boldsymbol{\chi}_k\|_2^2 \\ &\quad + \frac{\rho_2}{2}\|\mathbf{A}_2\mathbf{p}_k - \mathbf{s}_k + \boldsymbol{\mu}_k\|_2^2 - \frac{\rho_2}{2}\|\boldsymbol{\mu}_k\|_2^2 \\ &\quad + \frac{\rho_3}{2}\|\mathbf{A}_3\mathbf{p}_k - \mathbf{c}_k - \mathbf{b}_k + \boldsymbol{\nu}_k\|_2^2 - \frac{\rho_3}{2}\|\boldsymbol{\nu}_k\|_2^2 \end{aligned} \tag{54}$$

where $\boldsymbol{\chi}_k$, $\boldsymbol{\mu}_k$, and $\boldsymbol{\nu}_k$ are scaled Lagrange multipliers, and $\rho_1, \rho_2, \rho_3 > 0$ denote penalty parameters. The formulation of (54) plays a fundamental role in the scaled ADPM [27], we denote $\mathbf{p}_k^l$, $\mathbf{a}_k^l$, $\mathbf{s}_k^l$, $\mathbf{b}_k^l$, $\boldsymbol{\chi}_k^l$, $\boldsymbol{\mu}_k^l$, $\boldsymbol{\nu}_k^l$, ρ_1^l, ρ_2^l, and ρ_3^l as estimates of parameters at the lth iteration, and the iteration steps of the ADPM are given as follows.

Step 1: Update $\mathbf{a}_k$ by solving the following problem:

$$\min_{\mathbf{a}_k}\ \|\mathbf{A}_1\mathbf{p}_k^l - \mathbf{a}_k + \boldsymbol{\chi}_k^l\|_2^2 \quad \text{s.t.}\quad \mathbf{a}_k \in \mathbf{D}_{a,k} \tag{55}$$

which can be split into $N_{a,k} = |\mathbf{\Omega}_{a,k}|$ subproblems, and be solved parallelly, where $|\mathbf{\Omega}_{a,k}|$ is defined as the size of $\mathbf{\Omega}_{a,k}$. The ith $(i = 1, \ldots, N_{a,k})$ subproblem is

$$\min_{a_{i,k}}\ \left(\mathbf{p}^l_{\mathbf{\Omega}_{a,k}(i),k}(3) - a_{i,k} + \chi_{i,k}^l\right)^2 \quad \text{s.t.}\quad a_{i,k} \geq H_{\min} \tag{56}$$

where $\mathbf{\Omega}_{a,k}(i)$ denotes the ith element of the set $\mathbf{\Omega}_{a,k}$, $\chi_{i,k}^l$ is the ith element of the vector $\boldsymbol{\chi}_k^l$.

The closed-form solution of problem (56) at the lth iteration is

$$a_{i,k}^{l+1} = \begin{cases} H_{\min}, & \text{if } \mathbf{p}^l_{\mathbf{\Omega}_{a,k}(i),k}(3) + \chi_{i,k}^l < H_{\min} \\ \mathbf{p}^l_{\mathbf{\Omega}_{a,k}(i),k}(3) + \chi_{i,k}^l, & \text{else.} \end{cases} \tag{57}$$

Step 2: Update $\mathbf{s}_k$ by solving problem (58)

$$\min_{\mathbf{s}_k}\ \|\mathbf{A}_2\mathbf{p}_k^l - \mathbf{s}_k + \boldsymbol{\mu}_k^l\|_2^2 \quad \text{s.t.}\quad \mathbf{s}_k \in \mathbf{D}_{s,k}. \tag{58}$$

Note that problem (58) can be decomposed into $N_{s,k} = |\mathbf{\Omega}_{s,k}|$ subproblems, which can be solved parallelly. The ith $(i = 1, \ldots, N_{s,k})$ subproblem is

$$\min_{\mathbf{s}_{i,k}}\ \|\mathbf{p}_{j1,k}^l - \mathbf{p}_{j2,k}^l - \mathbf{s}_{i,k} + \boldsymbol{\mu}_{i,k}^l\|_2^2 \quad \text{s.t.}\quad \|\mathbf{s}_{i,k}\|_2 \geq d_{\text{col}} \tag{59}$$

where $(j1, j2) = \mathbf{\Omega}_{s,k}(i)$, $\mathbf{s}_{i,k}$ is the ith block of the vector $\mathbf{s}_k$. The closed-form solution of (59) is

$$\mathbf{s}_{i,k}^{l+1} = \begin{cases} \dfrac{\max(d_1, d_{\text{col}})}{d_1}(\mathbf{p}_{j1,k}^l - \mathbf{p}_{j2,k}^l + \boldsymbol{\mu}_{i,k}^l) \\ d_1 = \|\mathbf{p}_{j1,k}^l - \mathbf{p}_{j2,k}^l + \boldsymbol{\mu}_{i,k}^l\|_2. \end{cases} \tag{60}$$

Step 3: Update $\mathbf{b}_k$ by solving the following problem:

$$\min_{\mathbf{b}_k}\ \|\mathbf{A}_3\mathbf{p}_k^l - \mathbf{c}_k - \mathbf{b}_k + \boldsymbol{\nu}_k^l\|_2^2 \quad \text{s.t.}\quad \mathbf{b}_k \in \mathbf{D}_{b,k}. \tag{61}$$

Similarly, we divide problem (61) into $N_{b,k} = |\mathbf{\Omega}_{b,k}|$ subproblems and solve them parallelly. The ith $(i = 1, \ldots, N_{b,k})$ subproblem is

$$\min_{\mathbf{b}_{i,k}}\ \|\mathbf{p}_{j1,k}^l - \mathbf{c}_{j2,k} - \mathbf{b}_{i,k} + \boldsymbol{\nu}_{i,k}^l\|_2^2 \quad \text{s.t.}\quad \|\mathbf{b}_{i,k}\|_2 \geq r_{j2} \tag{62}$$

where $(j1, j2) \in \mathbf{\Omega}_{b,k}$, and $\mathbf{b}_{i,k}$ are ith block of $\mathbf{b}_k$.

The closed-form solution to problem (62) is given by

$$\mathbf{b}_{i,k}^{l+1} = \begin{cases} \dfrac{\max(d_2, r_{j2})}{d_2}(\mathbf{p}_{j1,k}^l - \mathbf{c}_{j2,k} + \boldsymbol{\nu}_{i,k}^l) \\ d_2 = \|\mathbf{p}_{j1,k}^l - \mathbf{c}_{j2,k} + \boldsymbol{\nu}_{i,k}^l\|_2. \end{cases} \tag{63}$$

Step 4: Update $\mathbf{p}_k$ by solving problem (64)

$$\begin{aligned} \min_{\mathbf{p}_k}\ & f(\mathbf{p}_k) + \frac{\rho_1^l}{2}\|\mathbf{A}_1\mathbf{p}_k - \mathbf{a}_k^{l+1} + \boldsymbol{\chi}_k^l\|_2^2 \\ & + \frac{\rho_2^l}{2}\|\mathbf{A}_2\mathbf{p}_k - \mathbf{s}_k^{l+1} + \boldsymbol{\mu}_k^l\|_2^2 \\ & + \frac{\rho_3^l}{2}\|\mathbf{A}_3\mathbf{p}_k - \mathbf{c}_k - \mathbf{b}_k^{l+1} + \boldsymbol{\nu}_k^l\|_2^2 \\ \text{s.t.}\quad & \mathbf{p}_{n,k} \in \mathbf{D}_{n,k},\ n = 1, 2, \ldots, N. \end{aligned} \tag{64}$$

Although (64) is a nonconvex problem [42], the variable $\mathbf{p}_k = [\mathbf{p}_{1,k}^T, \mathbf{p}_{2,k}^T, \ldots, \mathbf{p}_{N,k}^T]$ can be divided into N blocks, each one with a convex constraint. Therefore, we can solve problem (64) with **Algorithm 1** for a stationary point at the lth iteration.

Step 5: Update penalty variables ρ_1, ρ_2, and ρ_3 as follows:

$$\rho_1^{l+1} = \begin{cases} \rho_1^l, & \text{if } \triangle r_a^{l+1} \leq \epsilon_{1,a} \triangle r_a^l \\ \rho_1^l \epsilon_{2,a}, & \text{else} \end{cases} \tag{65}$$

Algorithm 3 The Scaled ADPM

Input:

Initialize variables: $\mathbf{p}_k^l$, $\boldsymbol{\chi}_k^l$, $\boldsymbol{\mu}_k^l$ and $\boldsymbol{\nu}_k^l$;

Initialize parameters: ρ_1^l, ρ_2^l, ρ_3^l, and let $l = 0$;

repeat

1. Update primal variable $\mathbf{a}_k^{l+1}$ by (57);
2. Update primal variable $\mathbf{s}_k^{l+1}$ by (60);
3. Update primal variable $\mathbf{b}_k^{l+1}$ by (63);
4. Update primal variable $\mathbf{p}_k^{l+1}$ by **Algorithm 1**;
5. Update penalty parameters $\{\rho_1^{l+1}, \rho_2^{l+1}, \rho_3^{l+1}\}$ by (65), (66), and (67);
6. Update dual variables $\{\boldsymbol{\chi}_k^{l+1}, \boldsymbol{\mu}_k^{l+1}, \boldsymbol{\nu}_k^{l+1}\}$ by (68), (69), and (70);
7. Let $l = l + 1$;

until *A predifined stopping criterion is achieved*;

Return: $\mathbf{p}_k = \mathbf{p}_k^l$, $\mathbf{a}_k = \mathbf{a}_k^l$, $\mathbf{s}_k = \mathbf{s}_k^l$, and $\mathbf{b}_k = \mathbf{b}_k^l$.

Algorithm 4 The Time-Varying CSM

1. Calculate $\boldsymbol{\Omega}_{a,k}$, $\boldsymbol{\Omega}_{s,k}$, and $\boldsymbol{\Omega}_{b,k}$ according to (5);

if $\boldsymbol{\Omega}_{a,k}$, $\boldsymbol{\Omega}_{s,k}$, *and* $\boldsymbol{\Omega}_{b,k}$ *are empty sets* **then**

2.1 Solve (40) by **Algorithm 1**;

else

2.2 Remove the constraints corresponding to the empty sets question (38);

2.3 Introduce auxiliary variables for positive security constraints to construct problem (53);

2.4 Solve (53) by **Algorithm 3**;

end

Return: $\mathbf{p}_k$.

$$\rho_2^{l+1} = \begin{cases} \rho_2^l, & \text{if } \triangle r_s^{l+1} \le \epsilon_{1,s} \triangle r_s^l \\ \rho_2^l \epsilon_{2,s}, & \text{else} \end{cases} \tag{66}$$

$$\rho_3^{l+1} = \begin{cases} \rho_3^l, & \text{if } \triangle r_b^{l+1} \le \epsilon_{1,b} \triangle r_b^l \\ \rho_3^l \epsilon_{2,b}, & \text{else} \end{cases} \tag{67}$$

where $0 < \epsilon_{1,a}, \epsilon_{1,s}, \epsilon_{1,b} < 1$, and $\epsilon_{2,a}, \epsilon_{2,s}, \epsilon_{2,b} > 1$ but close to 1. $\triangle r_a^l = \|\mathbf{A}_1\mathbf{p}_k^l - \mathbf{a}_k^l\|_2$, $\triangle r_s^l = \|\mathbf{A}_2\mathbf{p}_k^l - \mathbf{s}_k^l\|_2$, and $\triangle r_b^l = \|\mathbf{A}_3\mathbf{p}_k^l - \mathbf{c}_k - \mathbf{b}_k^l\|_2$ are residuals corresponding to constraints in (53).

Step 6: Update scaled dual variables as follows:

$$\boldsymbol{\chi}_k^{l+1} = \begin{cases} \widetilde{\boldsymbol{\chi}}_k^{l+1}, & \text{if } \chi_{\max}^{l+1} \le \varpi_a \\ \widetilde{\boldsymbol{\chi}}_k^{l+1}/\chi_{\max}^{l+1}, & \text{else} \end{cases} \tag{68}$$

$$\boldsymbol{\mu}_k^{l+1} = \begin{cases} \widetilde{\boldsymbol{\mu}}_k^{l+1}, & \text{if } \mu_{\max}^{l+1} \le \varpi_s \\ \widetilde{\boldsymbol{\mu}}_k^{l+1}/\mu_{\max}^{l+1}, & \text{else} \end{cases} \tag{69}$$

$$\boldsymbol{\nu}_k^{l+1} = \begin{cases} \widetilde{\boldsymbol{\nu}}_k^{l+1}, & \text{if } \nu_{\max}^{l+1} \le \varpi_b \\ \widetilde{\boldsymbol{\nu}}_k^{l+1}/\nu_{\max}^{l+1}, & \text{else} \end{cases} \tag{70}$$

where $\widetilde{\boldsymbol{\chi}}_k^{l+1} = \frac{\rho_1^l}{\rho_1^{l+1}}\boldsymbol{\chi}_k^l + \mathbf{A}_1\mathbf{p}_k^{l+1} - \mathbf{a}_k^{l+1}$, $\widetilde{\boldsymbol{\mu}}_k^{l+1} = \frac{\rho_2^l}{\rho_2^{l+1}}\boldsymbol{\mu}_k^l + \mathbf{A}_2\mathbf{p}_k^{l+1} - \mathbf{s}_k^{l+1}$, $\widetilde{\boldsymbol{\nu}}_k^{l+1} = \frac{\rho_3^l}{\rho_3^{l+1}}\boldsymbol{\nu}_k^l + \mathbf{A}_3\mathbf{p}_k^{l+1} - \mathbf{c}_k - \mathbf{b}_k^{l+1}$, $\chi_{\max}^{l+1}$, $\mu_{\max}^{l+1}$ and $\nu_{\max}^{l+1}$ represent the elements with the largest absolute values in the vectors $\widetilde{\boldsymbol{\chi}}_k^{l+1}$, $\widetilde{\boldsymbol{\mu}}_k^{l+1}$, and $\widetilde{\boldsymbol{\nu}}_k^{l+1}$, respectively. ϖ_a, ϖ_s, and ϖ_b are sufficiently large positive numbers.

If $\rho_1^{l+1} = \rho_1^l$, $\rho_2^{l+1} = \rho_2^l$, and $\rho_3^{l+1} = \rho_3^l$, the ADPM falls into the classic ADMM [27]. The idea behind the penalty and dual-parameters update is to try to keep the primal residual norms converging to zero. Specifically, if $\triangle r_a^l$ does not decrease with iterations, a larger ρ_1^{l+1} is utilized to make $\triangle r_a^l$ approaches zero to find a feasible solution. This operation not only improves the convergence of the classic ADMM but also makes the ADPM less dependent on the initial point [43]. As far as we know, the global convergence of the ADPM for general nonconvex problems is still an open problem [44]. On the other hand, our numerical results suggest that the ADPM can converge from any starting point. Toward understanding the numerical behavior, we provide the following weak converge result for ADPM, where the bounded of multipliers and the diminishing of $\|\mathbf{p}_k^{l+1} - \mathbf{p}_k^l\|_2$ are always observed numerically.

Theorem 1: Suppose $\{\rho_1^l, \rho_2^l, \rho_3^l\}$ are bounded, and $\lim_{l\to\infty} \|\mathbf{p}_k^{l+1} - \mathbf{p}_k^l\|_2 = 0$. Then, the sequence $\{\mathbf{p}_k^l, \mathbf{a}_k^l, \mathbf{s}_k^l, \mathbf{b}_k^l\}$ converges to limit points $\{\mathbf{p}_k^*, \mathbf{a}_k^*, \mathbf{s}_k^*, \mathbf{b}_k^*\}$, which are Karush–Kuhn–Tucker (KKT) points of the original problem (38).

Proof: See the Appendix.

Repeat steps 1–6 until some terminal conditions are satisfied, e.g., a maximum iteration number. We summarize the iteration steps of the scaled ADPM in **Algorithm 3**. Note that all kinds of security constraints are considered in **Algorithm 3**, which is the most complex case. In practice, we need to first determine which security constraints work, and then use **Algorithm 3** to solve problem (53) after removing the inactive constraints, which can improve the efficiency of the algorithm. Combining the two cases mentioned earlier, we give the time-varying CSM, as shown in **Algorithm 4**.

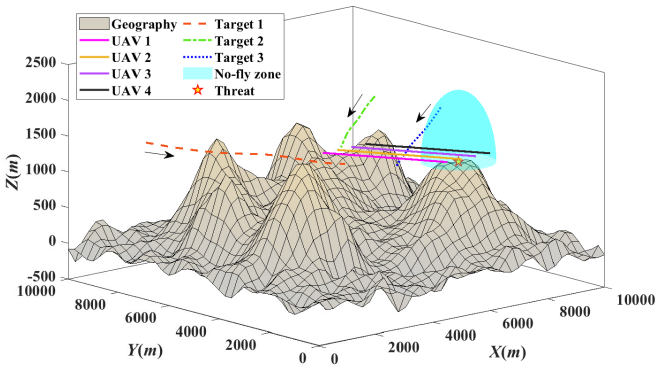

Fig. 5. Trajectories of multitarget and unoptimized paths of UAVs in scenario 1.

V. Simulation Results

This section presents simulation results to evaluate the performance of the proposed CSM in different scenarios. A 3-D area of $[0, 10\,000]$ m $\times$ $[0, 10\,000]$ m $\times$ $[0, 2000]$ m is investigated in scenario 1, where a team of $N = 4$ UAVs is used to cooperatively track a number of $Q = 3$ targets, as is shown in Fig. 5. The number of obstacle points and threats are set to $N_B = 1600$ and $N_T = 1$,

TABLE I
PARAMETERS FOR MTT IN SCENARIO 1

Parameter	Symbol	Value
Target 1's initial position	$\mathbf{x}_{1,1}^{p}$	$[1,\ 8,\ 1.5]^T$ km
Target 1's initial velocity	$\mathbf{x}_{1,1}^{v}$	$[20,\ -30,\ -1]^T$ m/s
Target 2's initial position	$\mathbf{x}_{2,1}^{p}$	$[9,\ 8,\ 1.5]^T$ km
Target 2's initial velocity	$\mathbf{x}_{2,1}^{v}$	$[-30,\ -25,\ -1]^T$ m/s
Target 3's initial position	$\mathbf{x}_{3,1}^{p}$	$[9.5,\ 6,\ 1.5]^T$ km
Target 3's initial velocity	$\mathbf{x}_{3,1}^{v}$	$[-30,\ -17,\ -1]^T$ m/s
Fusion time interval	T_0	2 s
Process noise intensity	τ_q	0.1 $\mathrm{m}^2/\mathrm{s}^3$

TABLE II
PARAMETERS OF MULTI-UAV MOUNTED AOA SENSORS

Parameter	Symbol	Value
UAV 1's initial position	$\mathbf{p}_{1,1}$	$[4500, 0, 1700]^T$
UAV 2's initial position	$\mathbf{p}_{2,1}$	$[5000, 0, 1700]^T$
UAV 3's initial position	$\mathbf{p}_{3,1}$	$[5500, 0, 1700]^T$
UAV 4's initial position	$\mathbf{p}_{4,1}$	$[6000, 0, 1700]^T$
Maximum turning angle	$\alpha_{\max}^{n}$	40° m
Maximum velocity magnitude	$v_{\max}^{n}$	40 m/s
Minimum height	$H_{\min}$	10 m
Collision avoidance distance	d_{col}	100 m
Clearance distance	r_i	300 m for obstacle avoidance 500 m for target avoidance 1000 m for threat avoidance
3dB beamwidth for azimuth	θ_{3dB}	0.035 rad
3dB beamwidth for elevation	φ_{3dB}	0.0175 rad

respectively. The initial states for multiple targets in the KF and dynamic parameters are shown in Table I. For simplicity, we set the initial velocity of each UAV to $[-15,\ 25,\ 0]^T$ m/s, the remaining parameters of multi-UAV mounted on AOA sensors are given in Table II. We assume the RCS of target q w.r.t. UAV n is $\kappa_{n,q,k} = 1\ \mathrm{m}^2$, $\forall n, q$. In this case, the signal-to-noise ratio (SNR) is only related to the geometry factor. The total flight time is 120 s for all experiments.

For the initialization of the NSPG method, it is usual to set $\lambda_{\min} = 10^{-5}$, $\lambda_{\max} = 10^{5}$, $\lambda_k^0 \in [\lambda_{\min}, \lambda_{\max}]$, $\sigma_1 = 0.1$, $\sigma_2 = 0.9$, $\varepsilon = 10^{-3}$, and $\delta = 10^{-4}$. A typical value for the nonmonotone parameter is $L = 10$. The initial point is set to be $\mathbf{p}_{n,k}^0 = \mathbf{p}_{n,k-1}$, $\forall n$. We initial the scaled dual vectors as zero vectors, $\varpi_a = \varpi_s = \varpi_b = 10^3$, $\rho_1^0 = \rho_2^0 = \rho_3^0 = 0.01$, $\epsilon_{1,a} = \epsilon_{1,s} = \epsilon_{1,b} = 0.95$, and $\epsilon_{2,a} = \epsilon_{2,s} = \epsilon_{2,b} = 1.05$ for initialization of the ADPM.

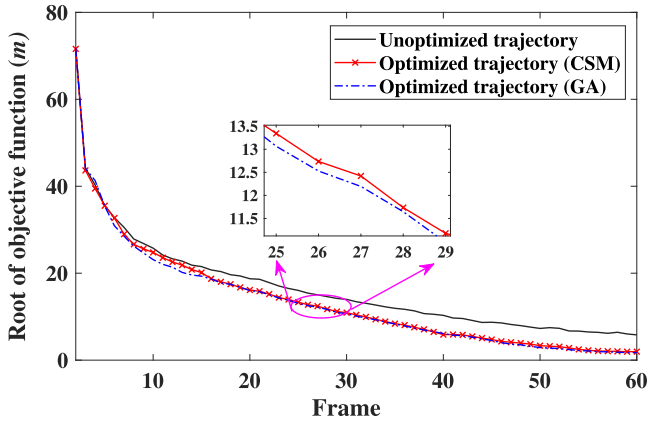

Fig. 6. Comparison of root of objective function values w.r.t. several methods in scenario 1.

A. Effectiveness of the Proposed CSM

In this section, numerical results are presented to demonstrate the MTT performance of the CSM in comparison with the conventional unoptimized method and the GA algorithm. The GA imitates natural selection and survival of the fittest, which is applied to find the optimal solution to the CTO problem in [20]. Since the GA is categorized as a global search method, it can be used to check the effectiveness of the CSM.

We first compare the passive MTT performance of these methods. Following the steps of the CSM listed in **Algorithm 4**, the root of objective function values of problem (38) corresponding to three methods are shown in Fig. 6. It is observed that the proposed CSM can achieve considerable MTT performance improvement over the conventional unoptimized method. In particular, the performance improvement is increasing as the frame elapses, and it reaches more than 50% in the last few frames. This is because both angular separation and targets' SNRs improve as the multi-UAV move toward multiple targets. Besides, the MTT performance of CSM and GA are nearly the same. Since there are no theoretical results on the iteration complexity of the ADPM, NSPG, and GA for the general nonconvex problem, as an alternative, we compare the runtime of the CSM and GA. The runtime comparison is carried out on a 2.9-GHz Intel Core i7-10700 processor with 32-GB RAM and averaged on the total number of frames in MATLAB 9.8.0 (2020a). The average runtime of the CSM is about 0.05 s, while that of the GA is 52.4 s. The GA costs the most time to find the optimal solution, due to its heuristic property. Combining the results in Fig. 6, we can conclude that the CSM achieves near-optimal MTT performance with much lower complexity than the GA.

B. Passive MTT Performance of the Two-Step Method

In this section, we test the effectiveness of the two-step tracking method. The root-mean-square error (RMSE) for target q is defined as follows:

$$R_{\mathrm{MSE},k}^{q} = \sqrt{\frac{1}{N_{\mathrm{mc}}}\sum_{m=1}^{N_{\mathrm{mc}}} \mathrm{tr}\left(\mathbf{\Lambda}^T \mathbf{x}_{q,k}^{\mathrm{err}} \mathbf{x}_{q,k}^{\mathrm{err}\ T} \mathbf{\Lambda}\right)} \tag{71}$$

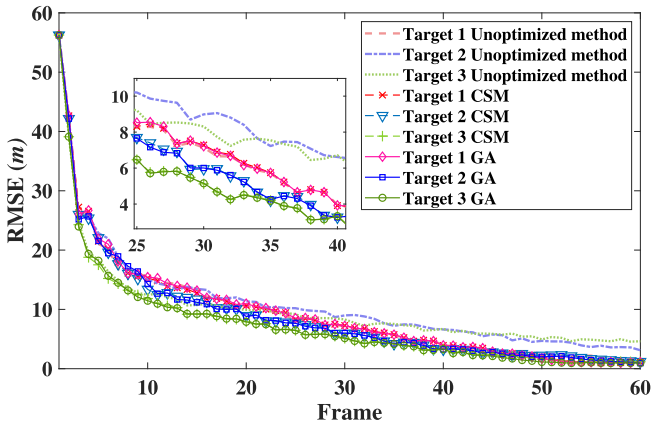

Fig. 7. RMSEs for multiple targets in scenario 1.

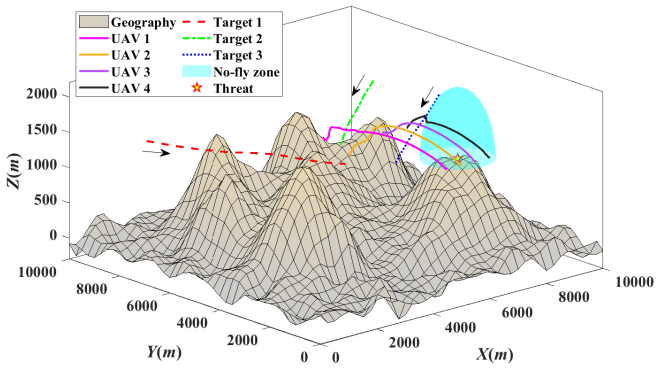

Fig. 8. CTO results w.r.t. the CSM in scenario 1.

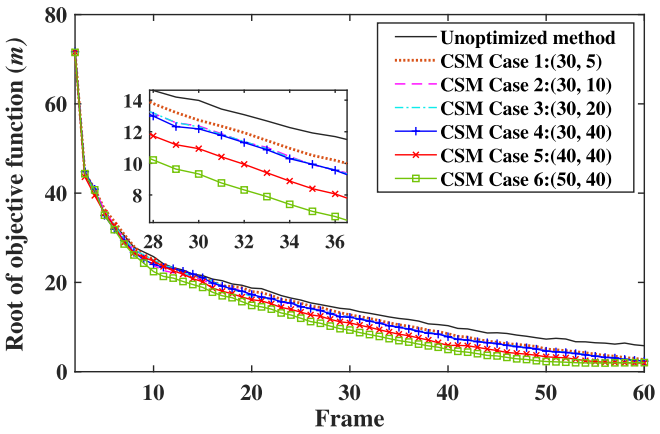

Fig. 9. Root of objective function comparison of several cases w.r.t. the CSM and the unoptimized method in scenario 1.

TABLE III
DISTANCES BETWEEN THREATS AND UAVS AT CERTAIN FRAMES

Frame	Threat-UAV Pair	Distance (m)
59, 60	(Target 2, UAV 2)	547, 521
56, 58, 59 60	(Target 3, UAV 4)	522, 537, 569
56, 57, 58, 59 60	(Target 3, UAV 3)	562, 558, 553, 559, 559
41, 42, 43, 44, 45	(Threat, UAV 4)	1071, 1064, 1065, 1074, 1084

where $N_{\mathrm{mc}} = 100$ represents the number of Monte Carlo trials. $\mathbf{x}_{q,k}^{\mathrm{err}} = \hat{\mathbf{x}}_{q,k}^{m} - \mathbf{x}_{q,k}$ denotes the estimation error, and $\hat{\mathbf{x}}_{q,k}^{m}$ is the state estimate at the mth trial. The RMSEs for multiple targets are depicted in Fig. 7.

From the results in Fig. 7, we see that RMSEs for multiple targets w.r.t. GA and CSM are nearly the same, which is consistent with the results in Fig. 6. The RMSE of target 1 is barely improved after the CTO process, while the RMSEs of targets 2 and 3 are significantly improved. This is due to the unoptimized linear trajectories moving toward target 1, which has an increasing SNR. After the CTO, UAVs 1 and 2 move toward target 1, and UAVs 3 and 4 gradually approach targets 2 and 3 (see Fig. 8). Therefore, the proposed CSM achieves a higher overall MTT accuracy than the unoptimized method by improving the tracking accuracy of targets 2 and 3 while maintaining the tracking accuracy of target 1.

C. Effects of Threat Avoidance on MTT Performance

The optimized trajectories of UAVs w.r.t. the CSM are shown in Fig. 8. We can see that multi-UAVs move toward multiple targets and the inter-UAV distances are increasing as time elapses. In this case, the SNRs of multiple targets and the angular separation of multi-UAV are continuously improved. This is consistent with the conclusions drawn from Fig. 6.

During the CTO process, obstacle avoidance constraints are activated at some frames, and the corresponding distances between obstacles/threats and UAVs are listed in Table III. The results in Table III depict that the CSM is capable to avoid targets/threats when the distance between the UAV and the target/threat may be less than the clearance distance.

D. Effects of Maneuver on MTT Performance

The maneuver capability of multi-UAV is affected by the maximum speed $v_{\max}^{n}$ and the maximum turning angle $\alpha_{\max}^{n}$. To explore the effects of $v_{\max}^{n}$ and $\alpha_{\max}^{n}$ on MTT performance. We consider six combinations of maximum speed and maximum turning angle, namely, $(v_{\max}^{n}, \alpha_{\max}^{n})$. The root objective function values corresponding to these cases are compared in Fig. 9.

In Fig. 9, cases 1–4 w.r.t. the CSM are used to verify the influence of the turning angle constraint on MTT performance, and cases 4–6 are used to verify the effect of speed constraint on MTT performance. In the first 20 frames, the tracking accuracy of case 1 is very close to that of the unoptimized method. This is because the initial speed (29.15 m/s) of the target is close to the maximum speed, and it is difficult to obtain an appropriate angular separation by a small turning angle (the CTO problem is similar to the steering control problem in this case). Comparing case 1 with case 2, we can observe the MTT performance can be further improved by increasing the maximum turning angle, but if the optimal turning angle corresponding to the maximum speed is less than the maximum turning angle, the MTT accuracy cannot be improved by increasing the maximum turning angle (see cases 2 to 4). Cases 4–6 show that the effect of maximum speed

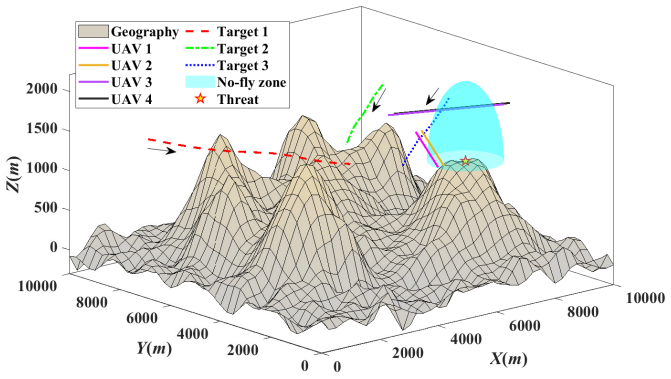

Fig. 10. Trajectories of multitarget and unoptimized paths of UAVs in scenario 2.

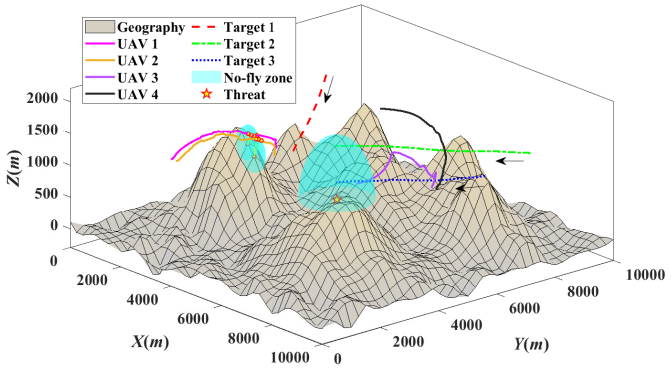

Fig. 11. Optimized trajectories of UAVs in scenario 2.

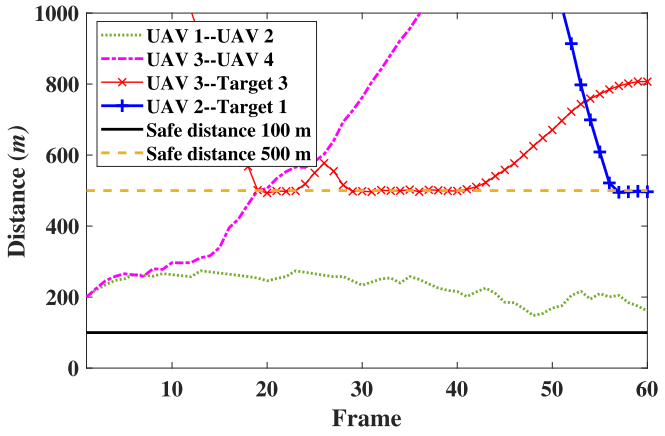

Fig. 12. Interdistances between two pairs of UAVs in scenario 2.

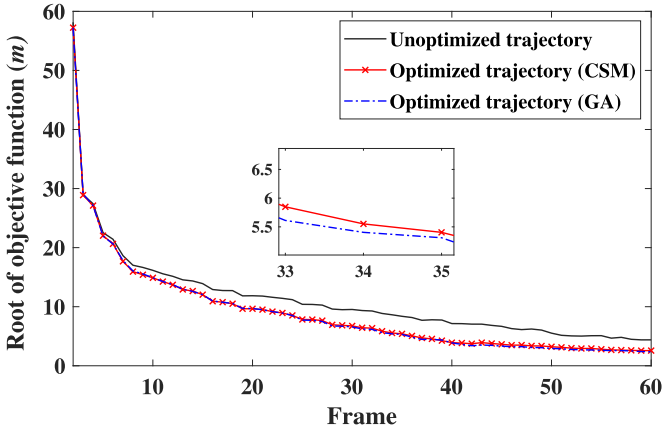

Fig. 13. Comparison of root of objective function values w.r.t. several methods in scenario 2.

constraint on MTT performance is relatively obvious. This is because the UAV is far from the target at frame $k = 1$, and the SNR is relatively low. In these cases, multiple UAVs should fly toward multitarget to improve the SNR, thus improving the tracking accuracy. In addition, when the UAV approaches the target, the performance improvement may become smaller since the UAV needs to keep a safe distance from the target (see cases 5 and 6 after frames 55).

E. Effects of Collision Avoidance on MTT Performance

In Fig. 5, the distance between every two adjacent UAVs is 500 m at frame $k = 1$. In this scenario, the collision avoidance is inactive during the CTO process, since multiple UAVs pull away from each other to obtain a good angular separation. In this section, we consider another scenario in Fig. 10, where the initial distance between adjacent UAVs is set to be smaller. The initial positions of UAVs 1 to 4 are set to be $[4, 0, 1.7]^T$ km, $[4.2, 0, 1.7]^T$ km, $[9.7, 4, 1.6]^T$ km, and $[9.9, 4, 1.6]^T$ km, respectively. The initial velocity of UAVs 1 and 2 are set to be $[15, 25, 0]^T$ m/s, and the initial velocity of UAVs 3 and 4 are set to be $[-25, 10, 0]^T$ m/s.

In scenario 2, the collision avoidance constraints may be activated in the first few frames. The optimized trajectories of multi-UAV are shown in Fig. 11. We can observe that UAVs 1 and 2 gradually approach target 1 while maintaining a safe distance (300 m) from obstacles during the CTO process. The obstacle avoidance constraints are activated at frames $k = 47 \sim 50$, during which a distance of at least 300 m was maintained between UAVs 1 and 2 and the obstacle points. Note that these obstacles also act as occlusions, that is, a payload sensor may not receive AOA measurements from a target when it is occluded. The occlusion leads to performance degradation of the estimator for the CM, due to the reduction in the number of measurements received. Fortunately, the obstacles did not obscure the UAV's light of sight in Fig. 11. UAVs 3 and 4 move toward targets 2 and 3 at the first few frames, then they chase these targets after the UAV and the target gets closer.

The inter-UAV distances between two UAVs that may collide and distances between UAVs and targets that may trigger threat avoidance constraints are shown in Fig. 12. It can be seen that any two adjacent UAVs are able to keep a safe distance, and UAVs 2 and 3 maintain a safe distance from targets 1 and 3, respectively. At frames $k = 20, 36$, the distances between UAV 3 and target 3 are slightly less than 500 m, due to the error between the predicted state provided by the KF and the true state of target 3.

The comparison of the objective functions between the proposed CSM, GA, and the unoptimized algorithm in scenario 2 is shown in Fig. 13. We can observe that the proposed CSM still achieves considerable MTT performance improvement

over the unoptimized method and provides nearly the same performance as the GA. It is consistent with the conclusions drawn from Fig. 6. The performance improvement of the proposed CSM in scenario 2 is smaller than that in scenario 1 since the SNRs of multiple targets are higher in scenario 2 than that in scenario 1.

VI. Conclusion

A 3-D CTO framework is proposed in this article, which collects measurements from the AOA sensors mounted on multi-UAV, constructs the tracks of multiple targets, and computes the control commands for the UAVs. A two-step tracking method is applied in MTT to provide the prior information for CTO, and the PC-CRLB is adopted as the tracking performance measure. We represent the height, collision, and obstacle/target/threat avoidance as time-varying security constraints, and then formulate the CTO as a nonconvex problem subjected to the security and dynamic constraints. The CSM is presented to solve the resulting CTO problem. If all security constraints are inactive, the CTO can be simplified as a nonconvex problem with convex dynamic constraints, which can be solved by the NSPG method. Conversely, we present an ADPM to solve the CTO problem with some positive security constraints. The ADPM introduces auxiliary vectors to decouple the complicated constraints and separates the CTO into several subproblems and tackles them alternately, while locally adjusting the penalty factor at each iteration. Numerical examples demonstrate that the CSM provides a significant improvement in passive MTT performance in comparison with the unoptimized method. Besides, the CSM achieves near-optimal performance with much lower complexity compared with the GA. The CSM is myopic since it only considers the MTT performance in the next time step. A more effective way would be the multistep CTO since each optimization will affect the possible trajectories over several future fusion intervals. The multistep CTO problem will be considered as our further work.

Appendix
Proof of Theorem 1

Since the penalty parameters $\{\rho_1^l, \rho_2^l, \rho_3^l\}$ are bounded, from (65) to (67), we have $\lim_{l\to\infty}\|\boldsymbol{\chi}_k^{l+1}-\boldsymbol{\chi}_k^l\|_2=0$, $\lim_{l\to\infty}\|\boldsymbol{\mu}_k^{l+1}-\boldsymbol{\mu}_k^l\|_2=0$, and $\lim_{l\to\infty}\|\boldsymbol{\nu}_k^{l+1}-\boldsymbol{\nu}_k^l\|_2=0$. This implies $\lim_{l\to\infty}\|\mathbf{A}_1\mathbf{p}_k^l-\mathbf{a}_k^l\|_2=0$, $\lim_{l\to\infty}\|\mathbf{A}_2\mathbf{p}_k^l-\mathbf{s}_k^l\|_2=0$, and $\lim_{l\to\infty}\|\mathbf{A}_3\mathbf{p}_k^l-\mathbf{c}_k-\mathbf{b}_k^l\|_2=0$. Since $\lim_{l\to\infty}\|\mathbf{p}_k^{l+1}-\mathbf{p}_k^l\|_2=0$,[2] and $\mathbf{D}_{n,k}$ is a bounded set, we have $\lim_{l\to\infty}\mathbf{p}_k^l=\mathbf{p}_k^*$, $\mathbf{A}_1\mathbf{p}_k^*=\mathbf{a}_k^*$, $\mathbf{A}_2\mathbf{p}_k^*=\mathbf{s}_k^*$, and $\mathbf{A}_3\mathbf{p}_k^*-\mathbf{c}_k=\mathbf{b}_k^*$. The first-order optimality condition of subproblem (55) is

$$\mathbf{0}=-\rho_1^l\left(\mathbf{A}_1\mathbf{p}_k^l-\mathbf{a}_k^{l+1}+\boldsymbol{\chi}_k^l\right)+\boldsymbol{\xi}_k^{a,l}\odot\nabla\mathbf{g}_a\left(\mathbf{a}_k^{l+1}\right) \tag{A.1}$$

where $\boldsymbol{\xi}_k^{a,l}$ is the dual variable of subproblem (55) at the l iteration, $\mathbf{g}_a(\mathbf{a}_k^{l+1})$ are the constraint functions w.r.t. the $\mathbf{D}_{a,k}$, and $\odot$ denotes the Hadamard product. According to (A.1), $\mathbf{A}_1\mathbf{p}_k^*=\mathbf{a}_k^*$, and $\lim_{l\to\infty}\|(\mathbf{A}_1\mathbf{p}_k^l-\mathbf{a}_k^l)\|_2=0$, we have

$$\mathbf{0}=\lim_{l\to\infty}-\rho_1^l\boldsymbol{\chi}_k^l+\boldsymbol{\xi}_k^{a,l}\odot\nabla\mathbf{g}_a\left(\mathbf{a}_k^{l+1}\right)$$

$$=-\rho_1^*\mathbf{A}_1^T\boldsymbol{\chi}_k^*+\boldsymbol{\xi}_k^{a*}\odot\mathbf{A}_1^T\nabla\mathbf{g}_a\left(\mathbf{a}_k^*\right) \tag{A.2}$$

where $\boldsymbol{\xi}_k^{a*}$ is the optimal dual variable. Similarly, the first-order optimality conditions of subproblems (58), (61), and (64) are given by

$$\mathbf{0}=-\rho_2^*\mathbf{A}_2^T\boldsymbol{\mu}_k^*+\boldsymbol{\xi}_k^{s*}\odot\mathbf{A}_2^T\nabla\mathbf{g}_s\left(\mathbf{s}_k^*\right) \tag{A.3}$$

$$\mathbf{0}=-\rho_3^*\mathbf{A}_3^T\boldsymbol{\nu}_k^*+\boldsymbol{\xi}_k^{b*}\odot\mathbf{A}_3^T\nabla\mathbf{g}_b(\mathbf{b}_k^*) \tag{A.4}$$

$$\mathbf{0}=\nabla f\left(\mathbf{p}_k^*\right)+\rho_1^*\mathbf{A}_1^T\boldsymbol{\chi}_k^*+\rho_2^*\mathbf{A}_2^T\boldsymbol{\mu}_k^*+\rho_3^*\mathbf{A}_3^T\boldsymbol{\nu}_k^*+\boldsymbol{\xi}_k^{p*}\odot\nabla\mathbf{g}_p\left(\mathbf{p}_k^*\right) \tag{A.5}$$

where $\boldsymbol{\xi}_k^{s*}$, $\boldsymbol{\xi}_k^{b*}$, and $\boldsymbol{\xi}_k^{p*}$ are optimal dual variables. $\mathbf{g}_s(\mathbf{s}_k^{l+1})$, $\mathbf{g}_b(\mathbf{b}_k^{l+1})$, and $\mathbf{g}_p(\mathbf{p}_k^{l+1})$ denote the constraint functions w.r.t. the $\mathbf{D}_{s,k}$, $\mathbf{D}_{b,k}$, and $\mathbf{D}_k$, respectively.

The Karush–Kuhn–Tucker (KKT) conditions of the original problem (38) are

$$\mathbf{0}=\nabla f(\mathbf{p}_k)+\boldsymbol{\upsilon}_k^p\odot\nabla\mathbf{g}_p(\mathbf{p}_k)+\boldsymbol{\upsilon}_k^a\odot\mathbf{A}_1^T\nabla\mathbf{g}_a(\mathbf{p}_k)+\boldsymbol{\upsilon}_k^s\odot\mathbf{A}_2^T\nabla\mathbf{g}_s(\mathbf{p}_k)+\boldsymbol{\upsilon}_k^b\odot\mathbf{A}_3^T\nabla\mathbf{g}_b(\mathbf{p}_k) \tag{A.6}$$

$$\boldsymbol{\upsilon}_k^a\odot\mathbf{g}_a(\mathbf{A}_1^T\mathbf{p}_k)=\mathbf{0},\ \ \boldsymbol{\upsilon}_k^s\odot\mathbf{g}_s(\mathbf{A}_2^T\mathbf{p}_k)=\mathbf{0}$$

$$\boldsymbol{\upsilon}_k^b\odot\mathbf{g}_b(\mathbf{A}_3^T\mathbf{p}_k-\mathbf{c}_k)=\mathbf{0},\ \ \boldsymbol{\upsilon}_k^p\odot\mathbf{g}_p(\mathbf{p}_k)=\mathbf{0} \tag{A.7}$$

$$\mathbf{g}_p(\mathbf{p}_k)\preceq\mathbf{0},\ \ \mathbf{g}_a(\mathbf{A}_1\mathbf{p}_k)\preceq\mathbf{0}$$

$$\mathbf{g}_s(\mathbf{A}_2\mathbf{p}_k)\preceq\mathbf{0},\ \ \mathbf{g}_b(\mathbf{A}_3\mathbf{p}_k-\mathbf{c}_k)\preceq\mathbf{0}$$

$$\boldsymbol{\upsilon}_k^p\succeq\mathbf{0},\ \ \boldsymbol{\upsilon}_k^a\succeq\mathbf{0},\ \ \boldsymbol{\upsilon}_k^s\succeq\mathbf{0},\ \ \boldsymbol{\upsilon}_k^b\succeq\mathbf{0} \tag{A.8}$$

$$\mathbf{A}_1\mathbf{p}_k=\mathbf{a}_k,\ \ \mathbf{A}_2\mathbf{p}_k=\mathbf{s}_k,\ \ \mathbf{A}_3\mathbf{p}_k-\mathbf{c}_k=\mathbf{b}_k. \tag{A.9}$$

From (A.2)–(A.5), the KKT conditions are satisfied by setting $\mathbf{p}_k=\mathbf{p}_k^*$, $\mathbf{a}_k=\mathbf{a}_k^*$, $\mathbf{s}_k=\mathbf{s}_k^*$, $\mathbf{b}_k=\mathbf{b}_k^*$, $\boldsymbol{\upsilon}_k^a=\boldsymbol{\xi}_k^{a*}$, $\boldsymbol{\upsilon}_k^s=\boldsymbol{\xi}_k^{s*}$, $\boldsymbol{\upsilon}_k^b=\boldsymbol{\xi}_k^{b*}$, and $\boldsymbol{\upsilon}_k^p=\boldsymbol{\xi}_k^{p*}$.

[2] $\lim_{l\to\infty}\|\mathbf{p}_k^{l+1}-\mathbf{p}_k^l\|_2=0$ cannot ensure $\lim_{l\to\infty}\mathbf{p}_k^l=\mathbf{p}_k^*$ in some extreme cases, which is beyond the scope of this article.

References

[1] S. F. Abedin, M. S. Munir, N. H. Tran, Z. Han, and C. S. Hong, "Data freshness and energy-efficient UAV navigation optimization: A deep reinforcement learning approach," *IEEE Trans. Intell. Transp. Syst.*, vol. 22, no. 9, pp. 5994–6006, Sep. 2021.

[2] J. Chen, C. Du, Y. Zhang, P. Han, and W. Wei, "A clustering-based coverage path planning method for autonomous heterogeneous UAVs," *IEEE Trans. Intell. Transp. Syst.*, vol. 23, no. 12, pp. 25546–25556, Dec. 2022.

[3] H. V. Nguyen, H. Rezatofighi, B.-N. Vo, and D. C. Ranasinghe, "Online UAV path planning for joint detection and tracking of multiple radio-tagged objects," *IEEE Trans. Signal Process.*, vol. 67, no. 20, pp. 5365–5379, Oct. 2019.

[4] Y.-J. Chen, D.-K. Chang, and C. Zhang, "Autonomous tracking using a swarm of UAVs: A constrained multi-agent reinforcement learning approach," *IEEE Trans. Veh. Technol.*, vol. 69, no. 11, pp. 13702–13717, Nov. 2020.

[5] Y. Zeng, R. Zhang, and T. J. Lim, "Wireless communications with unmanned aerial vehicles: Opportunities and challenges," *IEEE Commun. Mag.*, vol. 54, no. 5, pp. 36–42, May 2016.

[6] J. Yan, H. Jiao, W. Pu, C. Shi, J. Dai, and H. Liu, "Radar sensor network resource allocation for fused target tracking: A brief review," *Inf. Fusion*, vols. 86–87, pp. 104–115, Oct. 2022.

[7] E. Tzoreff and A. J. Weiss, "Single sensor path design for best emitter localization via convex optimization," *IEEE Trans. Wireless Commun.*, vol. 16, no. 2, pp. 939–951, Feb. 2017.

[8] H. Folker, M. Ritchie, A. Charlish, and H. Griffiths, "Sensor path planning using reinforcement learning," in *Proc. IEEE 23rd Int. Conf. Inf. Fusion (FUSION)*, Jul. 2020, pp. 1–8.

[9] F. Hoffmann, A. Charlish, M. Ritchie, and H. Griffiths, "Policy rollout action selection in continuous domains for sensor path planning," *IEEE Trans. Aerosp. Electron. Syst.*, vol. 57, no. 4, pp. 2247–2264, Aug. 2021.

[10] K. Dogancay, "Online optimization of receiver trajectories for scan-based emitter localization," *IEEE Trans. Aerosp. Electron. Syst.*, vol. 43, no. 3, pp. 1117–1125, Jul. 2007.

[11] K. Dogancay, H. Hmam, S. P. Drake, and A. Finn, "Centralized path planning for unmanned aerial vehicles with a heterogeneous mix of sensors," in *Proc. Int. Conf. Intell. Sensors, Sensor Netw. Inf. Process. (ISSNIP)*, Dec. 2009, pp. 91–96.

[12] S. A. A. Shahidian and H. Soltanizadeh, "Path planning for two unmanned aerial vehicles in passive localization of radio sources," *Aerosp. Sci. Technol.*, vol. 58, pp. 189–196, Nov. 2016.

[13] S. Uluskan, "Noncausal trajectory optimization for real-time range-only target localization by multiple UAVs," *Aerosp. Sci. Technol.*, vol. 99, Apr. 2020, Art. no. 105558.

[14] K. Doğançay, "UAV path planning for passive emitter localization," *IEEE Trans. Aerosp. Electron. Syst.*, vol. 48, no. 2, pp. 1150–1166, Apr. 2012.

[15] E. Tzoreff and A. J. Weiss, "Path design for best emitter location using two mobile sensors," *IEEE Trans. Signal Process.*, vol. 65, no. 19, pp. 5249–5261, Oct. 2017.

[16] M. L. Hernandez, "Optimal sensor trajectories in bearings-only tracking," in *Proc. 7th Int. Conf. Inf. Fusion*, vol. 2, 2004, pp. 893–900.

[17] C. Shi, X. Dai, Y. Wang, J. Zhou, and S. Salous, "Joint route optimization and multidimensional resource management scheme for airborne radar network in target tracking application," *IEEE Syst. J.*, vol. 16, no. 4, pp. 6669–6680, Dec. 2022.

[18] X. Lu, W. Yi, and L. Kong, "Joint online route planning and resource optimization for multitarget tracking in airborne radar systems," *IEEE Syst. J.*, vol. 16, no. 3, pp. 4198–4209, Sep. 2022.

[19] Y. Xiang, M. Akcakaya, S. Sen, D. Erdogmus, and A. Nehorai, "Target tracking via recursive Bayesian state estimation in cognitive radar networks," *Signal Process.*, vol. 155, pp. 157–169, Feb. 2019.

[20] R. Tharmarasa, T. Kirubarajan, and T. Lang, "Joint path planning and sensor subset selection for multistatic sensor networks," in *Proc. IEEE Symp. Comput. Intell. Secur. Defense Appl.*, Jul. 2009, pp. 1–8.

[21] F. Koohifar, A. Kumbhar, and I. Guvenc, "Receding horizon multi-UAV cooperative tracking of moving RF source," *IEEE Commun. Lett.*, vol. 21, no. 6, pp. 1433–1436, Jun. 2017.

[22] P. Zhan, D. W. Casbeer, and A. L. Swindlehurst, "A centralized control algorithm for target tracking with UAVs," in *Proc. Conf. Rec. 39th Asilomar Conf. Signals, Syst. Comput.*, 2005, pp. 1148–1152.

[23] P. Sarunic and R. Evans, "Hierarchical model predictive control of UAVs performing multitarget-multisensor tracking," *IEEE Trans. Aerosp. Electron. Syst.*, vol. 50, no. 3, pp. 2253–2268, Jul. 2014.

[24] S. Ragi and E. K. P. Chong, "UAV path planning in a dynamic environment via partially observable Markov decision process," *IEEE Trans. Aerosp. Electron. Syst.*, vol. 49, no. 4, pp. 2397–2412, Oct. 2013.

[25] S. Ragi and E. K. P. Chong, "Decentralized control of unmanned aerial vehicles for multitarget tracking," in *Proc. Int. Conf. Unmanned Aircr. Syst. (ICUAS)*, May 2013, pp. 260–268.

[26] S. Xu, K. Doğançay, and H. Hmam, "Distributed pseudolinear estimation and UAV path optimization for 3D AOA target tracking," *Signal Process.*, vol. 133, pp. 64–78, Apr. 2017.

[27] S. Boyd, N. Parikh, and E. Chu, *Distributed Optimization and Statistical Learning via the Alternating Direction Method of Multipliers*. New York, NY, USA: Now, 2011.

[28] I. Klein and Y. Bar-Shalom, "Tracking with asynchronous passive multisensor systems," *IEEE Trans. Aerosp. Electron. Syst.*, vol. 52, no. 4, pp. 1769–1776, Aug. 2016.

[29] D. Willner, C. Chang, and K. Dunn, "Kalman filter algorithms for a multi-sensor system," in *Proc. IEEE Conf. Decis. Control Including 15th Symp. Adapt. Processes*, Dec. 1976, pp. 570–574.

[30] K. L. Bell, C. J. Baker, G. E. Smith, J. T. Johnson, and M. Rangaswamy, "Cognitive radar framework for target detection and tracking," *IEEE J. Sel. Top. Signal Process.*, vol. 9, no. 8, pp. 1427–1439, Dec. 2015.

[31] E. G. Birgin, J. M. Martinez, and M. Raydan, "Nonmonotone spectral projected gradient methods on convex sets," *SIAM J. Optim.*, vol. 10, no. 4, pp. 1196–1211, 2000.

[32] L. D. Stone, R. L. Streit, T. L. Corwin, and K. L. Bell, *Bayesian Multiple Target Tracking*. Norwood, MA, USA: Artech House, 2013.

[33] C. Shi, Y. Wang, S. Salous, J. Zhou, and J. Yan, "Joint transmit resource management and waveform selection strategy for target tracking in distributed phased array radar network," *IEEE Trans. Aerosp. Electron. Syst.*, vol. 58, no. 4, pp. 2762–2778, Aug. 2022.

[34] D. Musicki, "Multi-target tracking using multiple passive bearings-only asynchronous sensors," *IEEE Trans. Aerosp. Electron. Syst.*, vol. 44, no. 3, pp. 1151–1160, Jul. 2008.

[35] C. Shi, L. Ding, F. Wang, S. Salous, and J. Zhou, "Joint target assignment and resource optimization framework for multitarget tracking in phased array radar network," *IEEE Syst. J.*, vol. 15, no. 3, pp. 4379–4390, Sep. 2021.

[36] M. A. Richards, *Fundamentals of Radar Signal Processing*. New York, NY, USA: McGraw-Hill, 2014.

[37] S. Challa, M. R. Morelande, D. Mušicki, and R. J. Evans, *Fundamentals of Object Tracking*. Cambridge, U.K.: Cambridge Univ. Press, 2011.

[38] C. T. Kelley, *Iterative Methods for Optimization*. Philadelphia, PA, USA: SIAM, 1999.

[39] J. Dai et al., "Composed resource optimization for multitarget tracking in active and passive radar network," *IEEE Trans. Geosci. Remote Sens.*, vol. 60, 2022, Art. no. 5119215.

[40] P. Krüsi, P. Furgale, M. Bosse, and R. Siegwart, "Driving on point clouds: Motion planning, trajectory optimization, and terrain assessment in generic nonplanar environments," *J. Field Robot.*, vol. 34, no. 5, pp. 940–984, Aug. 2017.

[41] S. Mehrotra, "On the implementation of a primal-dual interior point method," *SIAM J. Optim.*, vol. 2, no. 4, pp. 575–601, 1992.

[42] S. Boyd, S. P. Boyd, and L. Vandenberghe, *Convex Optimization*. Cambridge, U.K.: Cambridge Univ. Press, 2004.

[43] X. Yu, G. Cui, J. Yang, J. Li, and L. Kong, "Quadratic optimization for unimodular sequence design via an ADPM framework," *IEEE Trans. Signal Process.*, vol. 68, pp. 3619–3634, 2020.

[44] M. Hong, Z.-Q. Luo, and M. Razaviyayn, "Convergence analysis of alternating direction method of multipliers for a family of nonconvex problems," *SIAM J. Optim.*, vol. 26, no. 1, pp. 337–364, Jan. 2016.

Jinhui Dai was born in Zhangjiakou, China. He is currently pursuing the Ph.D. degree with the National Laboratory of Radar Signal Processing, Xidian University, Xi'an, China.

His research interests include collaborative resource allocation, trajectory optimization, and target tracking.

Wenqiang Pu (Member, IEEE) received the B.S. and Ph.D. degrees in electrical engineering from Xidian University, Xi'an, China, in 2013 and 2018, respectively.

From 2019 to 2020, he was a Post-Doctoral Researcher with the School of Science and Engineering, The Chinese University of Hong Kong (Shenzhen), Shenzhen, China. He is currently a Research Scientist with the Shenzhen Research Institute of Big Data, Shenzhen. His research interests include signal processing and optimization algorithms.

Junkun Yan (Senior Member, IEEE) was born in Sichuan, China, 1987. He received the B.S. and Ph.D. degrees in electronics engineering from Xidian University, Xi'an, China, in 2009 and 2015, respectively.

He is currently a Professor with the National Laboratory of Radar Signal Processing, Xidian University. He has authored and coauthored more than 70 scientific articles in refereed journals, including the IEEE TRANSACTIONS ON SIGNAL PROCESSING, *Information Fusion*, the IEEE TRANSACTIONS ON VEHICULAR TECHNOLOGY, *Signal Processing*, the IEEE TRANSACTIONS ON AEROSPACE AND ELECTRONIC SYSTEMS, and the IEEE SENSORS JOURNAL. His research interests include adaptive signal processing, target tracking, and radar resource allocation.

Dr. Yan was a recipient of the Excellent Doctoral Thesis Award from the Shannxi Institute of Electronics in 2017 and the Young Talent Fund of the China Association for Science and Technology in 2020. He is currently an Associate Editor of the IEEE TRANSACTIONS ON AEROSPACE AND ELECTRONIC SYSTEMS and *Signal Processing*.

Qingjiang Shi (Member, IEEE) received the Ph.D. degree in electronic engineering from Shanghai Jiao Tong University, Shanghai, China, in 2011.

From 2009 to 2010, he visited Prof. Z.-Q. (Tom) Luo's research group with the University of Minnesota at Twin Cities, Minneapolis, MN, USA. In 2011, he was a Research Scientist with Nokia Bell Laboratories, Shanghai. In 2012, he was with the School of Information and Science Technology, Zhejiang Sci-Tech University, Hangzhou, China. From 2016 to 2017, he was a Research Fellow with Iowa State University, Ames, IA, USA. Since 2018, he has been a Full Professor with the School of Software Engineering, Tongji University, Shanghai, China. He is also with the Shenzhen Research Institute of Big Data, Shenzhen, China. He has authored or coauthored more than 70 IEEE journals and filed about 30 national patents. His research interests include algorithm design and analysis with applications in machine learning, signal processing, and wireless networks.

Dr. Shi was a recipient of the Best Paper Award from the IEEE PIMRC'09 conference, the Shanghai Excellent Doctorial Dissertation Award in 2012, the National Excellent Doctoral Dissertation Nomination Award in 2013, the First Prize of Science and Technology Award from the China Institute of Communications in 2017, the Golden Medal at the 46th International Exhibition of Inventions of Geneva in 2018, the Huawei Outstanding Technical Achievement Award in 2021, and the Huawei Technical Cooperation Achievement Transformation Award (second prize) in 2022. He was an Associate Editor of the IEEE TRANSACTIONS ON SIGNAL PROCESSING.

Hongwei Liu (Senior Member, IEEE) received the M.Eng. and Ph.D. degrees in electronic engineering from Xidian University, Xi'an, China, in 1995 and 1999, respectively.

From 2001 to 2002, he was a Visiting Scholar with the Department of Electrical and Computer Engineering, Duke University, Durham, NC, USA. He is currently a Professor and the Director with the National Laboratory of Radar Signal Processing, Xidian University. His research interests include radar signal processing, radar automatic target recognition, adaptive signal processing, and cognitive radar.